Research Journal of Applied Sciences, Engineering and Technology 7(19): 4035-4055, 2014
DOI:10.19026/rjaset.7.765
ISSN: 2040-7459; e-ISSN: 2040-7467

Submitted: November 20, 2013 Accepted: December 29, 2013 Published: May 15, 2014

Research Article

Linearized Shallow-water Wave Theory of Tsunami Generation and Propagation by Three-dimensional Stochastic Seismic Bottom Topography

M.A. Omar, Khaled T. Ramadan and Allam. A. Allam
Department of Basic and Applied Science, College of Engineering and Technology, Arab Academy for Science, Technology and Maritime Transport, P.O. Box 1029, Abu Quir Campus, Alexandria, Egypt

Abstract: Tsunami generation and propagation resulting from lateral spreading of a stochastic seismic fault source model driven by two Gaussian white noises in the x- and y- directions are investigated. Tsunami waveforms within the frame of the linearized shallow water theory for constant water depth are analyzed analytically by transform methods (Laplace in time and Fourier in space) for the random sea floor uplift represented by a sliding Heaviside step function under the influence of two Gaussian white noise processes in the x- and y- directions. This model is used to study the tsunami amplitude amplification under the effect of the noise intensity and rise times of the stochastic fault source model. The amplification of tsunami amplitudes builds up progressively as time increases during the generation process due to wave focusing while the maximum wave amplitude decreases with time during the propagation process due to the geometric spreading and also due to dispersion. We derived and analyzed the mean and variance of the random tsunami waves as a function of the time evolution along the generation and propagation path.

Keywords: Bottom topography, Gaussian white noise, Itô integral, Laplace and Fourier transforms, shallow water theory, stochastic process, tsunami modeling

INTRODUCTION

The main reason for the generation and propagation of tsunamis is due to huge and rapid motion of the bottom of the ocean caused by an underwater earthquake over broad areas in comparison to water depth. Tsunami can also be caused by other undersea events such as volcanoes or landslides. However, in this study we focus on the purely seismic mechanism (i.e., underwater earthquake) which occurs most frequently in nature. The estimation of the tsunami waves caused by an underwater earthquake has become of great practical interest that attracts nowadays a lot of attention due in part to the intensive human activity in coastal areas. The evaluation of a local tsunami threat is useful to get a more effective measure for tsunami warning systems and for protection works. In recent years, there have been a number of subduction zone earthquakes that have generated unexpectedly large local tsunamis. For example, Papua New Guinea tsunami 17 July 1998, Sumatra earthquake and tsunami, 26 December 2004, Solomon Islands tsunami 2 April 2007, Samoa tsunami 29 September 2009 and the Chile tsunami 27 Feb 2010 and the Japan tsunami 11 March 2011. The massive destruction and loss of life associated with the recent tsunamis has underscored the need to develop and implement tsunami hazard mitigation measures. In recent years, significant advances have been made in developing mathematical models to describe the entire process of tsunami event generated by seismic seafloor deformation caused by an underwater earthquake (Abou-Dina and Hassan, 2006; Hassan, 2009; Zahibo *et al*., 2006). Numerical models based on the non-dispersive shallow water equations are often used to simulate tsunami propagation and runup (Hassan *et al*., 2010b; Titov and Synolakis, 1995). The sea bottom deformation following an underwater earthquake is a complex phenomenon. This is why, for theoretical or experimental studies, researchers have often used uniform bottom motions such as the vertical motion of a box. Most investigations of tsunami generation and propagation used integral solution (in space and time) for an arbitrary bed displacement based on a linearized description of wave motion in either a two- or three-dimensional fluid domain of uniform depth. The complexity of the integral solutions developed from the linear theory even for the simplest model of bed deformation prevented many authors from determining detailed wave behavior, especially near the source region. In reality the sea bottom deformation following an underwater earthquake are characterized by some

Corresponding Author: M.A. Omar, Department of Basic and Applied Science, College of Engineering and Technology, Arab Academy for Science, Technology and Maritime Transport, P.O. Box 1029, Abu Quir Campus, Alexandria, Egypt

rugosity. In practice, the available data about the geometries of the source model are always subject to some uncertainties. The missing information can be modeled by the inclusion of random effects. These circumstances have lead several authors to consider water wave propagation in random media (Gurevich *et al*., 1993; De Bouard *et al*., 2008; Nachbin, 2010). In this study, a stochastic model is proposed to describe the bottom irregularity and its effect on the generation and propagation of the tsunami waves. Moreover, the tsunami wave resulting from the random bottom source model is compared with the tsunami wave due to simplified uniform bottom topography in the form of sliding Heaviside step function. Using a stochastic source model, it is demonstrated that local tsunami amplitudes vary by as much as a factor of two or more, depending on the local bathymetry. If other earthquake source parameter such as focal depth is varied in addition to the slip distribution patterns, even greater uncertainty in local tsunami amplitude is expected.

Most previous research has modeled tsunami waves under the effect of deterministic source model. Hammack (1973) studied experimentally the generated waves by raising or lowering a box at one end of a channel. He considered two types of time histories: an exponential and a half-sine bed movement. Todorovska and Trifunac (2001) investigated the generation and propagation of waves by a slowly spreading uplift of the bottom in linearized shallow-water wave theory. They showed that the effects of the spreading of the ocean floor deformation (faulting, submarine slides or slumps) on the amplitudes and periods of the generated tsunamis are largest when the spreading velocity of uplift and the tsunami velocity are comparable. Todorovska *et al*. (2002) investigated tsunami generation by a slowly spreading uplift of the sea floor in the near field considering the effects of the source finiteness and directivity. They described mathematically various two-dimensional kinematic models of submarine slumps and slides as combinations of spreading constant or slopping uplift functions. There results show that for given constant water depth, the peak amplitude depends on the ratio of the spreading velocity of the sea floor to the long wavelength tsunami velocity, see Trifunac *et al*. (2002a). Hayir (2003) investigated the motion of a submarine block slide with variable velocities and its effects on the near-field tsunami amplitudes. He found that the amplitudes generated by the slide are almost the same as those created by its average velocity. Both Trifunac *et al*. (2002a) and Hayir (2003) used very simple kinematic source models represented by a Heaviside step functions for representing the generation of tsunami. Dutykh *et al*. (2006) studied the generation of long wave through the ocean by a moving bottom. They demonstrated the differences between the classical approach (passive generation) and the active generation under the effect of the bottom motion. Abou-Dina and Hassan (2006) constructed a numerical model of tsunami generation and propagation depending on a nonlinear theory under the effect of a variable bed displacement with constant water depth. They considered nonlinearities and omitted the linear effects of frequency dispersion. Dutykh and Dias (2007) studied theoretically the generated waves by multiplying the static deformations caused by slip along a fault by various time laws: instantaneous, exponential, trigonometric and linear. Kervella *et al*. (2007) performed a comparison between three-dimensional linear and nonlinear tsunami generation models. They observed very good agreement from the superposition of the wave profiles computed with the linear and fully nonlinear models. In addition, they found that the nonlinear shallow water model was not sufficient to model some of the waves generated by a moving bottom because of the presence of frequency dispersion. Moreover, they suggested that for most events the linear theory is sufficient. Hassan (2009) discussed the solution of the non-linear problem of propagation of waves generated in a homogeneous fluid, occupying an infinite channel, by the bounded motion of the bottom. He demonstrated that the predictions of the linear theory are in good agreement with those of the nonlinear theory for sufficiently small amplitude of the bottom's motion. Hassan *et al*. (2010a) investigated the tsunami evolution during its generation under the effect of the variable velocities of realistic submarine landslides based on a two-dimensional curvilinear slide model. They described the tsunami generation from submarine gravity mass flows in three stages: The first stage represented by a rapid curvilinear down and uplift faulting with rise time. The second stage represented by a unilaterally propagation in the positive direction to a significant length to produce curvilinear two-dimensional models represented by a depression slump and a displaced accumulation slide model. The last stage represented by the time variation in the velocity of the accumulation slide (block slide) by using transforms method. Ramadan *et al*. (2011) studied the nature of the tsunami build up and propagation during and after realistic curvilinear source models represented by a slowly uplift faulting and a spreading slip-fault model. They studied the tsunami amplitude amplification as a function of the spreading velocity and rise time. They also analyzed the normalized peak amplitude as a function of the propagated uplift length, width and the average depth of the ocean.

It is becoming widely recognized that bottom topography is irregular and difficult to predict and its aspects are best revealed through random source models which are more realistic, because sources of tsunamis are generally uncorrelated. Despite this, a few of the analytical and numerical studies considered stochastic source models for the investigation of the generation and propagation of tsunami waves. This is due to the complexity in the mathematical modeling and analysis of the stochastic case compared to the deterministic case. The main complexity in the

stochastic case arises from the difficulty in the derivation of the integral solution of the random profile. Probability of tsunami occurrence frequency on the coast of California was evaluated first by Wiegel (1970). Rascón and Villarreal (1975) worked a stochastic evaluation of possibility of tsunami hit on the Pacific coast of Mexico. Successively, similar studies have been undertaken to study the local property of the tsunami occurrence frequency. Nakamura (1986) considered an extended Poisson process in order to get a better fit to the exceedance probability of local tsunami. Geist (2002) determined the effect that rupture complexity, by way of different slip distribution patterns on the local tsunami wave field under the effect of stochastic source model. Geist (2005) developed rapid tsunami models to forecast far-field tsunami amplitudes from initial earthquake information using stochastic source model. De Bouard *et al*. (2008) studied the motion of the free surface of a body of fluid over a variable bottom, in a long wave asymptotic regime. They focused on the two-dimensional case, assuming that the bottom of the fluid region can be described by a stationary random process whose variations take place on short length scales and which are decorrelated on the length scale of the long waves. Craig *et al*. (2009) gave a new derivation and an analysis of long wave model equations for the dynamics of the free surface of a body of water over random variable bottom and illustrated several numerical simulations of nonlinear waves. They considered the case where the bottom is random with uniform statistical properties. They described the asymptotic regime of small amplitude long waves, for which the correlation length of the bottom is short compared to the wavelength. Manouzi and Seaïd (2009) developed an efficient numerical method for solving stochastic water waves of Wick type driven by white noise using combination of the Wiener-Itô chaos expansion with a Galerkin finite element method. Their method transforms the stochastic shallow water equations into a system of deterministic shallow water equations that are solved for each chaos coefficient in the solution expansion. Dutykh *et al*. (2011) estimated the maximum wave runup height on a random slope plain shore by solving the classical Nonlinear Shallow Water equations using finite volume schemes. They compared the results of the random bottom model with the more conventional approaches. Ramadan *et al*. (2014), we, considered the modeling of tsunami generation and propagation under the effect of stochastic submarine landslides and slumps spreading in two orthogonal directions.

In this study, we investigate the tsunami wave in the near and far field using the transform methods (Laplace in time and Fourier in space). A linearized solution for constant water depth is derived for a random sea floor uplift represented by a sliding Heaviside step function under the influence of two independent Gaussian white noise processes in the $x-$ and $y-$ directions. The appearance of the Gaussian white noise (an irregular stochastic process) in our bottom topography, leads to complications in the integrals resulting from the transform methods. These integrals were found to be of a stochastic type, which are not solvable as a Riemann or Lebesgue integral. Stochastic integrals are mainly classified as Itô or Stratonovich integrals, (Klebaner, 2005; Kloeden and Platen, 1992; Oksendal, 1995; Omar *et al*., 2009, 2011). In our work, we consider the resultant integrals in Itô sense, which can be solved by many numerical methods, see Kloeden and Platen (1992) and Omar *et al*. (2009, 2011). The objective of this study is to determine the effect of the stochastic bottom topography on the generation and propagation of the tsunami wave form and discuss aspects of tsunami generation that should be considered in developing this model as well as the propagation wave after the formation of the source model has been completed. Due to the stochastic nature of the bottom topography, the free surface elevation is considered to be a stochastic process, thus for each realization (sample path) of the bottom topography, there exist a corresponding realization for the free surface elevation. Studying just one realization of the bottom topography has no significance and cannot be used to analyze the behavior of all possible solutions. Therefore, we drive the mean and variance of the free surface elevation. Moreover, we study the fluid wave motion above the finite source, with different noise intensity of the stochastic source model for constant spreading velocity. The effects of dispersion due to the random bottom topography on the tsunami waveforms are treated analytically by means of measuring the variance and illustrating it graphically. In addition, we investigate the mean and the variance of the tsunami waveforms in the near and far fields during the time evolution.

MATHEMATICAL FORMULATION OF THE PROBLEM

Consider a three dimensional fluid domain Λ as shown in Fig. 1. It is supposed to represent the ocean above the fault area. It is bounded above by the free surface of the ocean $z = \eta\,(x, y, t)$ and below by the rigid ocean floor $z = -h\,(x, y) + \zeta(x, y, t)$, where $\eta\,(x, y, t)$ is the free surface elevation, $h\,(x, y)$ is the water depth and $\zeta\,(x, y, t)$ is the sea floor displacement function. The domain Λ is unbounded in the horizontal directions x and y and can be written as $\Lambda = R^2 \times [-h\,(x, y) + \zeta\,(x, y, t), \eta\,(x, y, t)]$. For simplicity, $h(x, y)$ is assumed to be a constant. Before the earthquake, the fluid is assumed to be at rest, thus the free surface and the solid boundary are defined by $z = 0$ and $z = -h$, respectively. Mathematically, these conditions can be written in the form of initial conditions: $\eta\,(x, y, 0) = \zeta(x, y, 0) = 0$. At time $t > 0$,

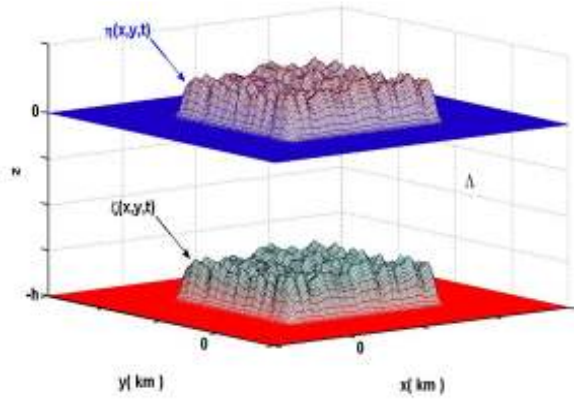

Fig. 1: Definition of the fluid domain and coordinate system for a very rapid movement of the assumed random source model

The bottom boundary moves in a prescribed manner which is given by $z = -h + \zeta(x, y, t)$. The deformation of the sea bottom is assumed to have all the necessary properties needed to compute its Fourier transform in x, y and its Laplace transform in t. The resulting deformation of the free surface $z = \eta\,(x, y, t)$ is to be found as part of the solution. It is assumed that the fluid is incompressible and the flow is irrotational. The former implies the existence of a velocity potential $\Phi\,(x, y, z, t)$ which fully describes the flow and the physical process. By definition of Φ, the fluid velocity vector can be expressed as $\vec{q} = \nabla\Phi$. Thus, the potential flow $\Phi\,(x, y, z, t)$ must satisfy the Laplace's equation:

$$\nabla^2\Phi(x, y, z, t) = 0 \; where \; (x, y, z) \in \Omega \qquad (1)$$

The potential $\Phi\,(x, y, z, t)$ must satisfy the following kinematic and dynamic boundary conditions on the free surface and the solid boundary, respectively:

$$\Phi_z = \eta_t + \Phi_x\,\eta_x + \Phi_y\,\eta_y \; on \; z = \eta(x, y, t) \qquad (2)$$

$$\Phi_z = \zeta_t + \Phi_x\,\zeta_x + \Phi_y\,\zeta_y \; on \; z = -\,h + \zeta(x, y, t) \qquad (3)$$

and

$$\Phi_t + \frac{1}{2}\,(\nabla\Phi)^2 + \; g\,\eta = 0 \; on \; z = \zeta(x, y, t) \qquad (4)$$

where, g is the acceleration due to gravity. As described above, the initial conditions are given by:

$$\Phi(x, y, z, 0) = \eta(x, y, 0) = \zeta(x, y, 0) = 0 \qquad (5)$$

Linear shallow water theory: Various approximations can be considered for the full water-wave equations. One is the system of nonlinear shallow-water equations that retains nonlinearity but no dispersion. Solving this problem is a difficult task due to the nonlinearities and the apriori unknown free surface. The concept of shallow water is based on the smallness of the ratio between water depth and wave length. In the case of tsunamis propagating on the surface of deep oceans, one can consider that shallow-water theory is appropriate because the water depth (typically several kilometers) is much smaller than the wave length (typically several hundred kilometers), which is reasonable and usually true for most tsunamis triggered by submarine earthquakes, slumps and slides, see Dutykh and Dias (2007) and Hammack (1973). Hence, the problem can be linearized by neglecting the nonlinear terms in the boundary conditions (2)-(4) and applying the boundary conditions on the non-deformed instead of the deformed boundary surfaces (i.e., $z = -h$ and on $z = 0$ instead of $z = -h + \zeta(x, y, t)$ and $z = \eta(x, y, t)$). The linearized problem in dimensional variables can be written as:

$$\nabla^2\Phi(x, y, z, t) = 0 \text{ where } (x, y, z) \in R^2 \times [-h, 0] \quad (6)$$

subjected to the following boundary conditions:

$$\Phi_z = \eta_t \text{ on } z = 0 \qquad (7)$$

$$\Phi_z = \zeta_t \text{ on } z = -h \qquad (8)$$

$$\Phi_t + \mathrm{g}\,\eta = 0 \text{ on } z = 0 \qquad (9)$$

The linearized shallow water solution can be obtained by the Fourier-Laplace transform.

Solution of the problem: Our interest is the resulting uplift of the free surface elevation $\eta\,(x, y, t)$. An analytical analysis is carried out to illustrate the generation and propagation of a tsunami for a given bed profile $\zeta\,(x, y, t)$. Mathematical modeling is carried out to obtain waves generated by vertical and lateral displacements of underwater earthquake using the combined Fourier-Laplace transform of the Laplace equation analytically. All our studies were taken into account constant depths for which the Laplace and Fast Fourier Transform (FFT) methods could be applied. The Eq. (6) to (9) can be solved by using the method of integral transforms. We apply the Fourier transform in (x, y):

$$\mathcal{F}_{xy}\{f(x, y)\} = f^{**}(k_1, k_2) = \int_{-\infty}^{\infty}\int_{-\infty}^{\infty} e^{-i(k_1 x + k_2 y)}\, f(x, y)\, dx\, dy$$

With its inverse transform:

$$\mathcal{F}^{-1}_{k_1 k_2}\{f^{**}(k_1, k_2)\} = f(x, y) = \frac{1}{(2\pi)^2}\int_{-\infty}^{\infty}\int_{-\infty}^{\infty} e^{i(x k_1 + y k_2)}\, f^{**}(k_1, k_2)\, dk_1\, dk_2$$

And the Laplace transform in time t:

$$\mathcal{L}\{g(t)\} = \hat{g}(s) = \int_0^\infty e^{-st}\, g(t)\, dt$$

Combining (7) and (9) yields the single free-surface condition:

$$\Phi_{tt}(x, y, 0, t) + g\, \Phi_z(x, y, 0, t) = 0 \quad (10)$$

After applying the transforms and using the property $\left[\mathcal{F}\left\{\frac{d^n f}{dx^n}\right\} = (i\,k)^n\, f^*(k)\right]$ and the initial conditions (5), Eq. (6), (8) and (10) become:

$$\hat{\Phi}^{**}_{zz}(k_1, k_2, z, s) - (k_1^2 + k_2^2)\, \hat{\Phi}^{**}(k_1, k_2, z, s) = 0 \quad (11)$$

$$\hat{\Phi}^{**}_z(k_1, k_2, -h, s) = s\, \hat{\zeta}^{**}(k_1, k_2, s) \quad (12)$$

$$s^2\, \hat{\Phi}^{**}(k_1, k_2, 0, s) + g\, \hat{\Phi}^{**}_z(k_1, k_2, 0, s) = 0 \quad (13)$$

The transformed free-surface elevation can be obtained from (9) as:

$$\hat{\eta}^{**}(k_1, k_2, s) = -\frac{s}{g}\, \hat{\Phi}^{**}(k_1, k_2, 0, s) = 0 \quad (14)$$

A general solution of (11) will be given by:

$$\hat{\Phi}^{**}(k_1, k_2, z, s) = A(k_1, k_2, s) \cosh(k\, z) + B(k_1, k_2, s) \sinh(k\, z) \quad (15)$$

where, $k = \sqrt{k_1^2 + k_2^2}$. The functions $A(k_1, k_2, s)$ and $B(k_1, k_2, s)$ can be easily found from the boundary conditions (12) and (13):

$$A(k_1, k_2, s)\cosh(k\, z) = -\frac{g\, s\, \hat{\zeta}^{**}(k_1, k_2, s)}{\cosh(k\, h)[s^2 + g\, k \tanh(k\, h)]} \quad (16)$$

$$B(k_1, k_2, s)\cosh(k\, z) = \frac{s^3\, \hat{\zeta}^{**}(k_1, k_2, s)}{k \cosh(k\, h)\, [s^2 + g\, k \tanh(k\, h)]} \quad (17)$$

Substituting (16) and (17) in the general solution (15) yields:

$$\hat{\Phi}^{**}(k_1, k_2, z, s) = -\frac{g\, s\, \hat{\zeta}^{**}(k_1, k_2, s)}{\cosh(k\, h)(s^2 + \omega^2)} \left(\cosh(k\, z) - \frac{s^2}{g\, k} \sinh(k\, z)\right) \quad (18)$$

where, $\omega = \sqrt{g\, k \tanh(k\, h)}$ is the circular frequency of the wave motion. The free surface elevation $\eta^{**}(k_1, k_2, s)$ can be obtained from (14) as:

$$\hat{\eta}^{**}(k_1, k_2, s) = \frac{s^2\, \hat{\zeta}^{**}(k_1, k_2, s)}{(s^2 + \omega^2) \cosh(kh)} \quad (19)$$

The circular frequency ω describes the dispersion relation of tsunamis and implies phase velocity $c = \frac{\omega}{k}$ and group velocity $U = \frac{d\omega}{dk}$. Hence, $c = \sqrt{\frac{g \tanh(kh)}{k}}$ and $U = \frac{1}{2}\, c\, \left(1 + \frac{2kh}{\sinh(2kh)}\right)$. Since, $k = \frac{2\,\pi}{\lambda}$, hence as $kh \to 0$, both $c \to \sqrt{gh}$ and $U \to \sqrt{gh}$, which implies that the tsunami velocity $v_t = \sqrt{gh}$ for wavelengths λ long compared to the water depth h. The free surface elevation $\eta\,(x, y, t)$ can be evaluated for a specified $\zeta\,(x, y, t)$ by obtaining its transform $\hat{\zeta}^{**}(k_1, k_2, s)$, then substituting it into (19) and inverting $\hat{\eta}^{**}(k_1, k_2, s)$ analytically to obtain $\eta^{**}(k_1, k_2, t)$ which is further converted to $\eta\,(x, y, t)$ by using double inverse Fourier Transform. The above linearized solution is known as the shallow water solution. We considered the stochastic source model for the sea floor displacement as a variable slip-fault, propagating unilaterally in the positive x −direction for time $0 \le t \le t^*$ with finite velocity v. In the y −direction, the model randomly propagate instantaneously.

The free surface elevation $\eta^{**}(k_1, k_2, t)$ can be evaluated by using inverse Laplace transform of $\eta^{**}(k_1, k_2, s)$ from the Convolution theorem as follows:

$$\eta^{**}(k_1, k_2, t) = \frac{1}{\cosh(kh)} \left[\zeta^{**}(k_1, k_2, t) - \omega 0 t \sin(\omega(t-u))\, \zeta^{**}k1, k2, u\, du\right] \quad (20)$$

The sea floor displacement is taken as:

$$\zeta(x, t) = \zeta_1(x, t) + \zeta_2(x, t) \quad (21)$$

where,

$$\zeta_1(x, t) = \zeta_0\, H\left(t - \frac{x}{v}\right) \quad (22)$$

$$\zeta_2(x, t) = \sigma_0\, \xi(x)\, \xi(y)\, H\left(t - \frac{x}{v}\right) \quad (23)$$

where, $H\,(x)$ represents the Heaviside function, ζ_0 denotes the initial uplift of the bottom topography, $\xi_x\,(x)$ and $\xi_y\,(y)$ denote two independent Gaussian white noise processes with a real valued parameter $\sigma_0 \ge 0$ that controls the strength of the induced noise and v is the rapture velocity of the stochastic bottom in the x −direction.

Laplace and Fourier transforms can now be applied to the bottom topography (21) to obtain:

$$\hat{\zeta}^{**}(k_1, k_2, s) = \hat{\zeta}_1^{**}(k_1, k_2, s) + \hat{\zeta}_2^{**}(k_1, k_2, s) \quad (24)$$

where,

$$\hat{\zeta}_1^{**}(k_1, k_2, s) = \frac{1 - e^{-ik_2 D}}{i\, k_2}\, \frac{\zeta_0}{s}\, \frac{1 - e^{-\left(ik_1 + \frac{s}{v}\right)L}}{ik_1 + \frac{s}{v}} \quad (25)$$

$$\hat{\zeta}_2^{**}(k_1, k_2, s) = \frac{\sigma_0}{s} \int_0^D e^{-ik_2 y}\, \xi(y)\, dy \int_0^L e^{-\left(ik_1 + \frac{s}{v}\right)x}\, \xi(x)\, dx \quad (26)$$

where, L and D are the propagated length and width of the stochastic bottom topography in the x-and y-direction, respectively.

The transformed free surface elevation, $\hat{\eta}^{**}(k_1, k_2, s)$, can be obtained by substituting (24) into (19) as:

$$\hat{\eta}^{**}(k_1, k_2, s) = \hat{\eta}_1^{**}(k_1, k_2, s) + \hat{\eta}_2^{**}(k_1, k_2, s) \tag{27}$$

where,

$$\hat{\eta}_i^{**}(k_1, k_2, s) = \frac{s^2\, \hat{\zeta}_i^{**}(k_1,k_2,s)}{(s^2+\omega^2)\cosh(kh)}\ i = 1, 2 \tag{28}$$

Substituting (26) into (28), yields:

$$\hat{\eta}_2^{**}(k_1, k_2, s) = \frac{\sigma_0\, s}{(s^2+\omega^2)\cosh(kh)} \int_0^D e^{-ik_2 y}\, \xi(y)\, dy \int_0^L e^{-\left(ik_1+\frac{s}{v}\right)x}\, \xi(x)\, dx \tag{29}$$

The free surface elevation $\eta_2^{**}(k_1, k_2, t)$ can be evaluated by using inverse Laplace transform of $\hat{\eta}_2^{**}(k_1, k_2, s)$ as follows:

$$\begin{aligned} \eta_2^{**}(k_1, k_2, t) &= \frac{\sigma_0}{\cosh(kh)} \int_0^D e^{-ik_2 y}\, \xi(y)\, dy \int_0^L e^{-ik_1 x} \cos\left(\omega\left(t-\frac{x}{v}\right)\right) H\left(t-\frac{x}{v}\right) \xi(x)\, dx \\ &= \frac{\sigma_0}{\cosh(kh)} \int_0^D e^{-ik_2 y}\, dW(y) \begin{cases} \int_0^L e^{-ik_1 x} \cos\left(\omega\left(t-\frac{x}{v}\right)\right) dW(x) & \text{for } t > t^* \\ \int_0^{tv} e^{-ik_1 x} \cos\left(\omega\left(t-\frac{x}{v}\right)\right) dW(x) & \text{for } t \le t^* \end{cases} \end{aligned} \tag{30}$$

where, $t^* = \frac{L}{v}$. The integrals in (30) are stochastic integrals that can be considered as Itô integrals. Such integrals can be solved by various methods, see Omar *et al*. (2011) and Kloeden and Platen (1992). The solution $\hat{\eta}_1^{**}(k_1, k_2, s)$ for $\hat{\zeta}_1^{**}(k_1, k_2, s)$ can be obtained from (25) and (28) as:

$$\hat{\eta}_1^{**}(k_1, k_2, s) = \frac{\zeta_0}{\cosh(k\, h)} \frac{1-e^{-ik_2 D}}{ik_2} \frac{v\left(1-e^{-(ik_1 v+s)t^*}\right)}{i\, k_1\, v+s} \tag{31}$$

That can be transformed to the time domain as:

$$\begin{aligned} \eta_1^{**}(k_1, k_2, t) &= \left(\frac{\zeta_0}{\cosh(kh)} \frac{1-e^{-ik_2 D}}{ik_2} \frac{v}{\omega^2-k_1^2\, v^2}\right) \times \\ &\begin{cases} \omega \sin(w\, t) + i\, k_1\, v \cos(w\, t) \\ -e^{-ik_1 v t^*}\left[\, \omega \sin\left(w(t-t^*)\right) + i\, k_1\, v \cos\left(w(t-t^*)\right)\right] & \text{for } t > t^* \\ \omega \sin(w\, t) + i\, k_1\, v \cos(w\, t) - i\, k_1\, v\, e^{-ik_1 v t} & \text{for } t \le t^* \end{cases} \end{aligned} \tag{32}$$

This completes the solution of the problem, $\eta^{**}(k_1, k_2, t) = \eta_1^{**}(k_1, k_2, t) + \eta_2^{**}(k_1, k_2, t)$, in the double Fourier transform domain.

Finally, $\eta\,(x, y, t)$ is evaluated using the Inverse Fast Fourier Transform (IFFT). The IFFT is a fast algorithm for efficient implementation of the Inverse Discrete Fourier Transform (IDFT). In this study, this inversion is done using the MATLAB IFFT algorithm.

In order to implement the algorithm efficiently, singularities should be removed by finite limits as follows:

- As $k \to 0$, implies $k_1 \to 0$, $k_2 \to 0$ and $\omega \to 0$, then $\eta_1^{**}(k_1, k_2, t)$ and $\eta_2^{**}(k_1, k_2, t)$ have the following limits:

$$\lim_{k\to 0} \eta_1^{**}(k_1, k_2, t) = \zeta_0\, v\, D \begin{cases} t^* & \text{for } t > t^* \\ t & \text{for } t \le t^* \end{cases}$$

$$\lim_{k\to 0} \eta_2^{**}(k_1, k_2, t) = \sigma_0\, W(D) \begin{cases} W(L) & \text{for } t > t^* \\ W(tv) & \text{for } t \le t^* \end{cases}$$

- As $k_1 \to 0$, implies $k = k_2$ and $\omega = \sqrt{\mathrm{g}\, k_2 \tanh(k_2 h)}$, then $\eta_1^{**}(k_1, k_2, t)$ and $\eta_2^{**}(k_1, k_2, t)$ have the following limits:

$$\lim_{k_1 \to 0} \eta_1^{**}(k_1, k_2, t) = \left(\frac{\zeta_0}{\cosh(k_2 h)} \frac{1 - e^{-ik_2 D}}{ik_2} \frac{v}{\omega} \right) \begin{cases} \sin(w\, t) - \sin\big(w(t - t^*)\big) & \text{for } t > t^* \\ \sin(w\, t) & \text{for } t \le t^* \end{cases}$$

$$\lim_{k_1 \to 0} \eta_2^{**}(k_1, k_2, t) = \frac{\sigma_0}{\cosh(k_1 h)} \int_0^D e^{-ik_2 y}\, dW(y) \begin{cases} \int_0^L \cos\left(\omega\left(t - \frac{x}{v}\right)\right) dW(x) & \text{for } t > t^* \\ \int_0^{tv} \cos\left(\omega\left(t - \frac{x}{v}\right)\right) dW(x) & \text{for } t \le t^* \end{cases}$$

- As $k_2 \to 0$, implies $k = k_1$ and $\omega = \sqrt{\mathrm{g}\, k_1 \tanh(k_1 h)}$, then $\eta_1^{**}(k_1, k_2, t)$ and $\eta_2^{**}(k_1, k_2, t)$ have the following limits:

$$\lim_{k_2 \to 0} \eta_1^{**}(k_1, k_2, t) = \left(\frac{\zeta_0}{\cosh(k_1 h)} \frac{v\, D}{\omega^2 - k_1^2 v^2} \right) \times \begin{cases} \omega \sin(w\, t) + i\, k_1\, v \cos(w\, t) \\ -e^{-ik_1 v t^*} \left[\omega \sin\big(w(t - t^*)\big) + i\, k_1\, v \cos\big(w(t - t^*)\big) \right], & \text{for } t > t^* \\ \omega \sin(w\, t) + i\, k_1\, v \cos(w\, t) - i\, k_1\, v\, e^{-ik_1 v t}, & \text{for } t \le t^* \end{cases}$$

$$\lim_{k_1 \to 0} \eta_2^{**}(k_1, k_2, t) = \frac{\sigma_0}{\cosh(kh)} \quad W(D) \begin{cases} \int_0^L e^{-ik_1 x} \cos\left(\omega\left(t - \frac{x}{v}\right)\right) dW(x) & t > t^* \\ \int_0^{tv} e^{-ik_1 x} \cos\left(\omega\left(t - \frac{x}{v}\right)\right) dW(x) & t \le t^* \end{cases}$$

Mathematical derivation of the mean and variance of the stochastic tsunami waveforms: The presence of Gaussian white noise in the model of the bottom topography, leads to randomness in the generated waveforms. These waveforms are considered to be a stochastic process, which has an infinite number of trajectories (realizations). All these trajectories are considered as solutions for our stochastic model, but some trajectories may be more probable than others. Thus, instead of dealing with only one of these trajectories, we drive mathematically the mean and variance of the stochastic tsunami waveforms to get a better insight of the overall behavior of the stochastic tsunami waveforms.

First, we derive the mean of the tsunami waveforms by expressing the transformed free surface elevation, $\hat{\eta}^{**}(k_1, k_2, s)$, using (29) and (31) as:

$$\hat{\eta}^{**}(k_1, k_2, s) = \hat{\eta}_1{}^{**}(k_1, k_2, s) + \hat{\alpha}^{**}(k_1, k_2, s) \int_0^D e^{-ik_2 y}\, dW(y) \int_0^L e^{-\left(ik_1 + \frac{s}{v}\right)x}\, dW(x) \tag{33}$$

where,

$$\hat{\alpha}^{**}(k_1, k_2, s) = \frac{\sigma_0}{\cosh(kh)} \frac{s}{(s^2 + \omega^2)} \tag{34}$$

Taking the expectation of (33) and using the property that the expectation of an Itô integral equals zero, see Oksendal (1995), yields:

$$E[\hat{\eta}^{**}(k_1, k_2, s)] = \hat{\eta}_1{}^{**}(k_1, k_2, s) \tag{35}$$

As the free surface elevation is a continues function in (x, y, t), thus the Fubini's theorem, see page 64 in Kloeden and Platen (1992), can be applied to obtain the mean of the tsunami waveforms:

$$E[\eta(x, y, t)] = \overline{\eta}(x, y, t) = \eta_1(x, y, t) \tag{36}$$

Second, to derive the variance of the tsunami waveforms we need to introducing the following operators:

- For a function $f(t_1, t_2)$, the double Laplace transform, $\mathcal{L}_{t_1 t_2}\{f(t_1, t_2)\}$ is defined by:

$$\mathcal{L}_{t_1 t_2}\{f(t_1, t_2)\} = \int_0^\infty \int_0^\infty e^{-(s_1 t_1 + s_2 t_2)} f(t_1, t_2)\, dt_1\, dt_2$$

- Let $\mathcal{F}_x\{f(x)\} = f^*(k) = \int_{-\infty}^{\infty} e^{-ikx} f(x)\, dx$ represents the Fourier transform of a function $f(x)$. By $\mathcal{F}_{x_c}\{f(x)\}$, we mean $\mathcal{F}_{x_c}\{f(x)\} = f^{\bullet}(k) = \int_{-\infty}^{\infty} e^{ikx} f(x)\, dx$.
- For a function $f(x, y)$, we define $\mathcal{F}_{xy_c}\{f(x, y)\}$ by:

$$\mathcal{F}_{xy_c}\{f(x, y)\} = f^{*\bullet}(k_1, k_2) = \int_{-\infty}^{\infty}\int_{-\infty}^{\infty} e^{-i(k_1 x - k_2 y)} f(x, y)\, dx\, dy$$

In addition to the previous operators, the following two lemmas are needed for the derivation of the variance.

Lemma 1:

$$\frac{1}{i\,k_1 - i\,k_2 + a} f^*(k_1)\,\overline{g^*(k_2)} = \mathcal{F}_{xy_c}\left\{\int_0^\infty e^{-au} f(x-u)\,\overline{g(y-u)}\, du\right\}, k_2 < k_1, a \geq 0$$

where $\overline{g}$ denotes the conjugate of the function g.

Proof:

$$\begin{aligned}
\mathcal{F}_{xy_c}\Big\{\int_0^\infty e^{-au} & f(x-u)\,\overline{g(y-u)}\, du\Big\} \\
&= \mathcal{F}_{xy_c}\Big\{\int_{-\infty}^{\infty} e^{-au} f(x-u)\,\overline{g(y-u)}\, H(u)\, du\Big\} \\
&= \mathcal{F}_{y_c}\Big\{\mathcal{F}_x\Big\{\int_{-\infty}^{\infty} f(x-u)\, e^{-au}\,\overline{g(y-u)}\, H(u)\, du\Big\}\Big\} \\
&= \mathcal{F}_{y_c}\Big\{f^*(k_1)\,\mathcal{F}_x\big\{e^{-ax}\,\overline{g(y-x)}\, H(x)\big\}\Big\} \\
&= f^*(k_1)\,\mathcal{F}_x\Big\{\int_{-\infty}^{\infty} e^{ik_2 y}\, e^{-ax}\,\overline{g(y-x)}\, H(x)\, dy\Big\} \\
&= f^*(k_1)\,\mathcal{F}_x\Big\{e^{-ax} H(x)\int_{-\infty}^{\infty} e^{ik_2 y}\,\overline{g(y-x)}\, dy\Big\} \\
&= f^*(k_1)\,\mathcal{F}_x\Big\{e^{-ax} H(x)\,\overline{\int_{-\infty}^{\infty} e^{-ik_2 y}\, g(y-x)\, dy}\Big\} \\
&= f^*(k_1)\,\mathcal{F}_x\Big\{e^{-ax} H(x)\,\overline{e^{-ik_2 x}\, g^*(k_2)}\Big\} \\
&= f^*(k_1)\,\overline{g^*(k_2)}\int_{-\infty}^{\infty} e^{-ik_1 x}\, e^{-ax} H(x)\, e^{ik_2 x}\, dx \\
&= f^*(k_1)\,\overline{g^*(k_2)}\int_0^\infty e^{-(ik_1 - ik_2 + a)x}\, dx \\
&= \frac{1}{i\,k_1 - i\,k_2 + a} f^*(k_1)\,\overline{g^*(k_2)}
\end{aligned} \tag{37}$$

Lemma 2:

$$\begin{aligned}
\mathcal{F}_{xx'_c}\,\mathcal{F}_{yy'_c}\,\mathcal{L}_{tt'} & \left\{\int_0^\infty f\left(x-u, y, t-\frac{u}{v}\right) H\left(t-\frac{u}{v}\right)\overline{g\left(x'-u, y', t'-\frac{u}{v}\right) H\left(t'-\frac{u}{v}\right)}\, du\right\} \\
&= \frac{1}{i\,k_1 - i\,k'_1 + \frac{s}{v} + \frac{s'}{v}}\,\hat{f}^{**}(k_1, k_2, s)\,\overline{\hat{g}^{**}(k'_1, k'_2, s')}
\end{aligned}$$

Proof:

$$\begin{aligned}
\mathcal{F}_{xx'_c}\,\mathcal{F}_{yy'_c}\,\mathcal{L}_{tt'} & \left\{\int_0^\infty f\left(x-u, y, t-\frac{u}{v}\right) H\left(t-\frac{u}{v}\right)\overline{g\left(x'-u, y', t'-\frac{u}{v}\right) H\left(t'-\frac{u}{v}\right)}\, du\right\} \\
&= \mathcal{F}_{xx'_c}\,\mathcal{F}_{yy'_c}\left\{\int_0^\infty \hat{f}(x-u, y, s)\, e^{-\frac{s}{v}u}\,\overline{\hat{g}(x'-u, y', s')\, e^{-\frac{s'}{v}u}}\, du\right\} \\
&= \mathcal{F}_{xx'_c}\left\{\int_0^\infty e^{-\left(\frac{s}{v}+\frac{s'}{v}\right)u}\,\hat{f}^*(x-u, k_2, s)\,\overline{\hat{g}^*(x'-u, k'_2, s')}\, du\right\}
\end{aligned} \tag{38}$$

Using Lemma 1, we obtain:

$$\begin{aligned}\mathcal{F}_{xx'_c}\,\mathcal{F}_{yy'_c}\,\mathcal{L}_{tt'}\quad & \left\{\int_0^{\infty} f\left(x-u,y,t-\frac{u}{v}\right) H\left(t-\frac{u}{v}\right)\overline{g\left(x'-u,y',t'-\frac{u}{v}\right) H\left(t'-\frac{u}{v}\right)}\, du\right\}\\ & = \frac{1}{i\,k_1 - i\,k'_1+\frac{s}{v}+\frac{s'}{v}}\,\hat{f}^{**}(k_1,k_2,s)\,\overline{\hat{g}^{**}(k'_1,k'_2,s')}\,.\end{aligned} \tag{39}$$

Let $R_{\Omega\overline{\Omega'}}(x,y,t,x',y',t') = E\left[\Omega(x,y,t)\,\overline{\Omega'(x',y',t')}\right]$ denotes the auto-correlation function of the process $\Omega(x,y,t)$. It can be shown that:

$$\mathcal{F}_{xx'_c}\,\mathcal{F}_{yy'_c}\,\mathcal{L}_{tt'}\{R_{\Omega\overline{\Omega'}}(x,y,t,x',y',t')\} = E\left[\widehat{\Omega}^{**}(k_1,k_2,s)\,\overline{\widehat{\Omega'}^{**}(k'_1,k'_2,s')}\right] \tag{40}$$

Assuming that $\widehat{\Omega}^{**}(k_1,k_2,s)$ is the difference between the transformed free surface elevation (33) and its mean (35):

$$\widehat{\Omega}^{**}(k_1,k_2,s) = \hat{\alpha}^{**}(k_1,k_2,s)\int_0^D e^{-ik_2y}\,dW(y)\int_0^L e^{-\left(ik_1+\frac{s}{v}\right)x}\,dW(x) \tag{41}$$

Then,

$$\begin{aligned}E\left[\widehat{\Omega}^{**}\quad (k_1,k_2,s)\overline{\widehat{\Omega'}^{**}(k'_1,k'_2,s')}\right]\\ = E\left[\left(\hat{\alpha}^{**}(k_1,k_2,s)\int_0^D e^{-ik_2y}\,dW(y)\int_0^L e^{-\left(ik_1+\frac{s}{v}\right)x}\,dW(x)\right)\times\right.\\ \left.\left(\overline{\hat{\alpha}^{**}(k'_1,k'_2,s')}\int_0^D e^{ik_2y}\,dW(y)\int_0^L e^{\left(ik'_1-\frac{s'}{v}\right)x}\,dW(x)\right)\right]\\ = \left(\hat{\alpha}^{**}(k_1,k_2,s)\,\overline{\hat{\alpha}^{**}(k'_1,k'_2,s')}\right)E\left[\left(\int_0^L e^{-\left(ik_1+\frac{s}{v}\right)x}\,dW(x)\right)\left(\int_0^L e^{\left(ik'_1-\frac{s'}{v}\right)x}\,dW(x)\right)\right]\times\\ E\left[\left(\int_0^D e^{-ik_2y}\,dW(y)\right)\left(\int_0^D e^{ik_2y}\,dW(y)\right)\right]\end{aligned} \tag{42}$$

Recalling the fact, see (Klebaner, 2005), that if $X(t)$ and $Y(t)$ are regular adapted processes, such that:

$$E\left[\int_0^T X^2(t)\,dt\right] < \infty \; and \; E\left[\int_0^T Y^2(t)\,dt\right] < \infty \tag{43}$$

Then, we have:

$$E\left[\left(\int_0^T X(t)\,dW(t)\right)\left(\int_0^T Y(t)\,dW(t)\right)\right] = \int_0^T E[X(t)\,Y(t)]\,dt \tag{44}$$

Hence (42) becomes:

$$\begin{aligned}E\left[\widehat{\Omega}^{**}(k_1,k_2,s)\quad \overline{\widehat{\Omega'}^{**}(k'_1,k'_2,s')}\right]\\ = \hat{\alpha}^{**}(k_1,k_2,s)\,\overline{\hat{\alpha}^{**}(k'_1,k'_2,s')}\int_0^D e^{-(ik_2-ik'_2)y}\,dy\int_0^L e^{-\left(ik_1-ik'_1+\frac{s}{v}+\frac{s'}{v}\right)x}\,dx\\ = \hat{\alpha}^{**}(k_1,k_2,s)\,\overline{\hat{\alpha}^{**}(k'_1,k'_2,s')}\,\frac{1-e^{-(ik_2-ik'_2)D}}{(i\,k_2-i\,k'_2)}\,\frac{1-e^{-\left(ik_1-ik'_1+\frac{s}{v}+\frac{s'}{v}\right)L}}{\left(i\,k_1-i\,k'_1+\frac{s}{v}+\frac{s'}{v}\right)}\\ = \frac{1}{(i\,k_2-i\,k'_2)}\,\frac{1}{\left(i\,k_1-i\,k'_1+\frac{s}{v}+\frac{s'}{v}\right)}\left[\hat{\alpha}^{**}(k_1,k_2,s)\,\overline{\hat{\alpha}^{**}(k'_1,k'_2,s')}\right.\\ -(\hat{\alpha}^{**}(k_1,k_2,s)\,e^{-ik_2D})\,\overline{(\hat{\alpha}^{**}(k'_1,k'_2,s')\,e^{-ik'_2D})}\\ -\left(\hat{\alpha}^{**}(k_1,k_2,s)\,e^{-\left(ik_1+\frac{s}{v}\right)L}\right)\overline{\left(\hat{\alpha}^{**}(k'_1,k'_2,s')\,e^{-\left(ik'_1+\frac{s'}{v}\right)L}\right)}\\ \left.-\left(\hat{\alpha}^{**}(k_1,k_2,s)\,e^{-\left(ik_1L+ik_2D+\frac{s}{v}L\right)}\right)\overline{\left(\hat{\alpha}^{**}(k'_1,k'_2,s')\,e^{-\left(ik'_1L+ik'_2D+\frac{s'}{v}L\right)}\right)}\right]\end{aligned} \tag{45}$$

Applying Lemma 2 to (45), we obtain:

$$
\begin{aligned}
&E\left[\widehat{\Omega}^{**}(k_1,k_2,s)\,\overline{\widehat{\Omega}'^{**}(k'_1,k'_2,s')}\,\right]\\
&=\mathcal{F}_{xx'_c}\,\mathcal{F}_{yy'_c}\,\mathcal{L}_{tt'}\Big\{\int_0^\infty\int_0^\infty \alpha\left(x-u,y-\tau,t-\tfrac{u}{v}\right)H\left(t-\tfrac{u}{v}\right)\overline{\alpha\left(x'-u,y'-\tau,t'-\tfrac{u}{v}\right)H\left(t'-\tfrac{u}{v}\right)}\,du\,d\tau\\
&-\int_0^\infty\int_0^\infty \alpha\left(x-u,y-D-\tau,t-\tfrac{u}{v}\right)H\left(t-\tfrac{u}{v}\right)\times\\
&\overline{\alpha\left(x'-u,y'-D-\tau,t'-\tfrac{u}{v}\right)H\left(t'-\tfrac{u}{v}\right)}\,du\,d\tau\\
&-\int_0^\infty\int_0^\infty \alpha\left(x-L-u,y-\tau,t-\tfrac{L+u}{v}\right)H\left(t-\tfrac{L+u}{v}\right)H\left(t-\tfrac{u}{v}\right)\times\\
&\overline{\alpha\left(x'-L-u,y'-\tau,t'-\tfrac{L+u}{v}\right)H\left(t'-\tfrac{L+u}{v}\right)H\left(t'-\tfrac{u}{v}\right)}\,du\,d\tau\\
&+\int_0^\infty\int_0^\infty \alpha\left(x-L-u,y-D-\tau,t-\tfrac{L+u}{v}\right)H\left(t-\tfrac{L+u}{v}\right)H\left(t-\tfrac{u}{v}\right)\times\\
&\overline{\alpha\left(x'-L-u,y'-D-\tau,t'-\tfrac{L+u}{v}\right)H\left(t'-\tfrac{L+u}{v}\right)H\left(t'-\tfrac{u}{v}\right)}\,du\,d\tau\Big\}
\end{aligned}
\tag{46}
$$

From (40) and (46), we can deduce that:

$$
\begin{aligned}
&R_{\Omega\overline{\Omega'}}(x,y,t,x',y',t')\\
&=\int_0^\infty\int_0^\infty \alpha\left(x-u,y-\tau,t-\tfrac{u}{v}\right)H\left(t-\tfrac{u}{v}\right)\overline{\alpha\left(x'-u,y'-\tau,t'-\tfrac{u}{v}\right)H\left(t'-\tfrac{u}{v}\right)}\,du\,d\tau\\
&-\int_0^\infty\int_0^\infty \alpha\left(x-u,y-D-\tau,t-\tfrac{u}{v}\right)H\left(t-\tfrac{u}{v}\right)\times\\
&\overline{\alpha\left(x'-u,y'-D-\tau,t'-\tfrac{u}{v}\right)H\left(t'-\tfrac{u}{v}\right)}\,du\,d\tau\\
&-\int_0^\infty\int_0^\infty \alpha\left(x-L-u,y-\tau,t-\tfrac{L+u}{v}\right)H\left(t-\tfrac{L+u}{v}\right)H\left(t-\tfrac{u}{v}\right)\times\\
&\overline{\alpha\left(x'-L-u,y'-\tau,t'-\tfrac{L+u}{v}\right)H\left(t'-\tfrac{L+u}{v}\right)H\left(t'-\tfrac{u}{v}\right)}\,du\,d\tau\\
&+\int_0^\infty\int_0^\infty \alpha\left(x-L-u,y-D-\tau,t-\tfrac{L+u}{v}\right)H\left(t-\tfrac{L+u}{v}\right)H\left(t-\tfrac{u}{v}\right)\times\\
&\overline{\alpha\left(x'-L-u,y'-D-\tau,t'-\tfrac{L+u}{v}\right)H\left(t'-\tfrac{L+u}{v}\right)H\left(t'-\tfrac{u}{v}\right)}\,du\,d\tau
\end{aligned}
\tag{47}
$$

Finally, the variance can be obtained by taking $x'=x$, $y'=y$ and $t'=t$ in the auto-correlation function (47):

$$
\begin{aligned}
Var[\Omega(x,y,t)] &= R_{\Omega\overline{\Omega}}(x,y,t)\\
&=\int_0^\infty\int_0^\infty \left|\alpha\left(x-u,y-\tau,t-\tfrac{u}{v}\right)H\left(t-\tfrac{u}{v}\right)\right|^2\,du\,d\tau\\
&-\int_0^\infty\int_0^\infty \left|\alpha\left(x-u,y-D-\tau,t-\tfrac{u}{v}\right)H\left(t-\tfrac{u}{v}\right)\right|^2\,du\,d\tau\\
&-\int_0^\infty\int_0^\infty \left|\alpha\left(x-L-u,y-\tau,t-\tfrac{L+u}{v}\right)H\left(t-\tfrac{L+u}{v}\right)H\left(t-\tfrac{u}{v}\right)\right|^2\,du\,d\tau\\
&+\int_0^\infty\int_0^\infty \left|\alpha\left(x-L-u,y-D-\tau,t-\tfrac{L+u}{v}\right)H\left(t-\tfrac{L+u}{v}\right)H\left(t-\tfrac{u}{v}\right)\right|^2\,du\,d\tau\\
&=\int_0^\infty\int_0^{t\,v} \left|\alpha\left(x-u,y-\tau,t-\tfrac{u}{v}\right)\right|^2\,du\,d\tau\\
&+\int_0^\infty\int_0^{t\,v} \left|\alpha\left(x-u,y-D-\tau,t-\tfrac{u}{v}\right)\right|^2\,du\,d\tau\\
&+\begin{cases}
\int_0^\infty\int_0^{t\,v-L} \left|\alpha\left(x-L-u,y-D-\tau,t-\tfrac{L+u}{v}\right)\right|^2\,du\,d\tau & \\
-\int_0^\infty\int_0^{t\,v-L} \left|\alpha\left(x-L-u,y-\tau,t-\tfrac{L+u}{v}\right)\right|^2\,du\,d\tau & for\ t>t^*\\
0 & for\ t\le t^*
\end{cases}
\end{aligned}
\tag{48}
$$

RESULTS AND DISCUSSION

In this section, we present numerical results to illustrate the nature of the tsunami build up and propagation during and after the uplift process of the assumed stochastic bottom topography. The numerical results demonstrate the waveform amplification resulting from source spreading in the $x-$direction and wave focusing in the near-field and the tsunami spreading in the far-field. When the source process is completed and for rapid lateral spreading, the displacement of the free surface above the source resembles the displacement of the ocean floor (Ramadan *et al*., 2011; Todorovska and Trifunac, 2001). For velocities of spreading smaller than v_t, the tsunami amplitudes in the direction of the source propagation become small with high frequencies. As the velocity of the spreading approaches v_t, the tsunami waveform has progressively larger amplitude, with high frequency content, in the direction of the slip spreading, (Ramadan *et al*., 2011; Todorovska and Trifunac, 2001). These large amplitudes are caused by wave focusing (i.e., during slow earthquakes). Examples of such slow earthquakes are the June 6, 1960, Chile earthquakes which ruptured as a series of earthquakes for about an hour, see Kanamori and Stewart (1972) and the February 21, 1978, Banda Sea earthquake, (Silver and Jordan, 1983).

Tsunami generally occurs due to vertical movement of the seafloor that vertically displaces the water column. Large vertical displacement of the sea bottom ground causes a corresponding large motion at the sea surface. The generation of tsunami by vertical displacements of the ocean floor depends on the characteristic size (length L and width D) of the displaced area and on the time t it takes to spread the motion over the entire source region. Therefore, researchers presented kinematic source models in the form of Heaviside functions to describe the generation of tsunamis, see Todorovska and Trifunac (2001), Trifunac and Todorovska (2002), Todorovska *et al*. (2002), Trifunac *et al*. (2002a, b) and Hammack (1973).

It is difficult to estimate, at present, how often the amplification may occur during actual faulting, sliding or slumping, because of the lack of detailed knowledge about the ground deformations in the source area of past tsunamis. Therefore, we constructed mathematically a reasonable random tsunami source model represented by a sliding Heaviside step function under the influence of two independent Gaussian white noise processes in the $x-$ and $y-$directions. Due to the stochastic nature of the tsunami waveforms, we mainly examine the mean and variance of the tsunami generation and propagation during time evolution.

Time-evolution during tsunami generation: The effects of variations of the uplift of the considered stochastic source model in the $x-$ and $y-$directions are studied as a function of time t on the generation of tsunamis. These effects are studied through the investigation of the generation of tsunamis by unilateral displacements of the ocean floor and under the effect of the normalized noise intensity $\sigma = \sigma_0/\zeta_0$. The velocity of the sea floor spreads, v, is chosen to be equal to the long wave tsunami velocity $v_t = \sqrt{gh}$, (i.e., maximum amplification). The tsunami waveforms generated for the stochastic source model with normalized noise intensity $\sigma = 0$ (deterministic case), 1 and 2 are illustrated in Fig. 2 to 4, respectively. These waveforms are generated at constant water depth $h = 2\,km$, propagated length $L = 100\,km$, source width $D = 50\,km$ at rise time $t = 0.25\,t^*, 0.5\,t^*, 0.75\,t^*$ and t^* where $t^* = \frac{L}{v}$ and $v = v_t$. It can be seen from these figures that the amplitude of the wave builds up progressively as t increases and the focusing and the amplification of tsunami amplitudes occur above the spreading edge of the source model Fig. 5.

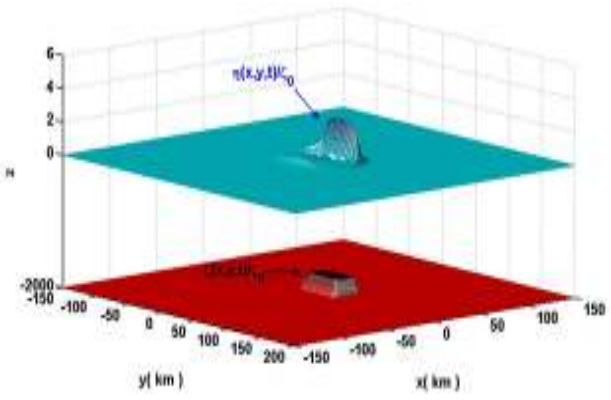

(a) $t = 0.25\,t^*$

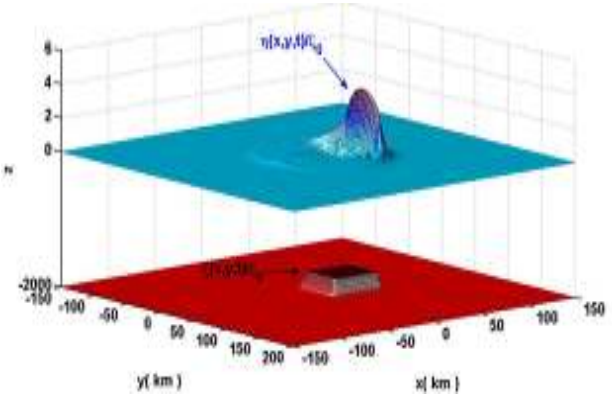

(b) $t = 0.5\,t^*$

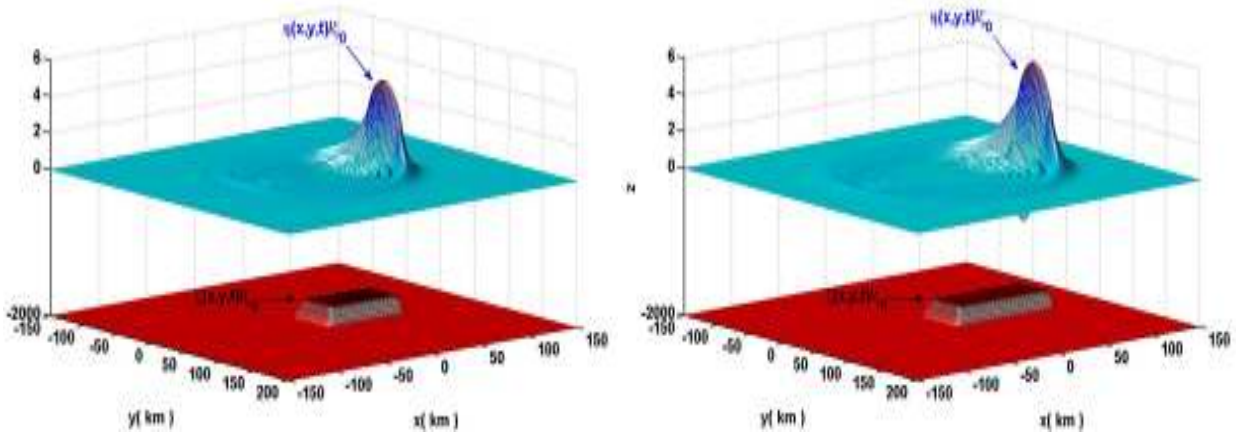

(c) $t = 0.75\ t^*$ (d) $t = \ t^*$

Fig. 2: Generation of the normalized tsunami waveforms, $\frac{\eta(x,y,t)}{\zeta_0}$, for different rise times at $\sigma = 0$, $L = 100\ km$, $D = 50\ km$, $t^* = \frac{L}{v}$ and $v = v_t$

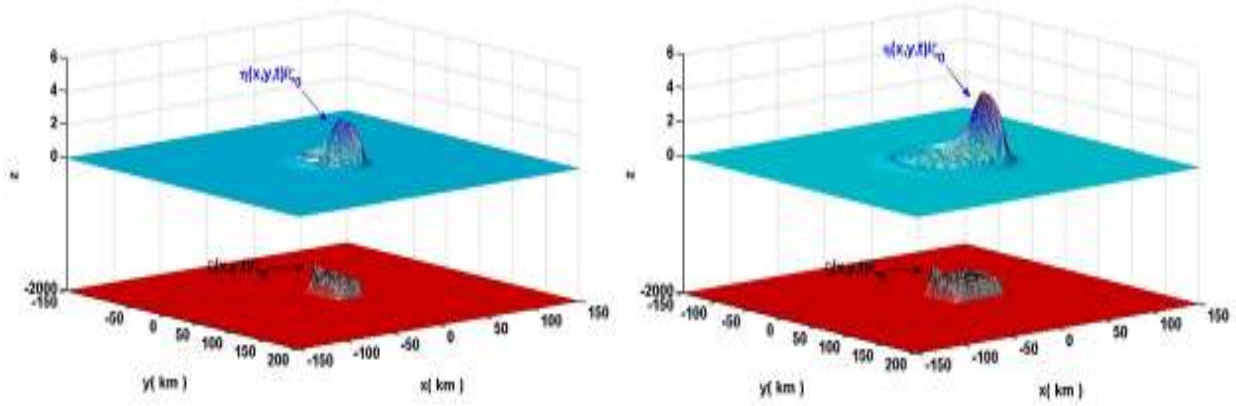

(a) $t = 0.25\ t^*$ (b) $t = 0.5\ t^*$

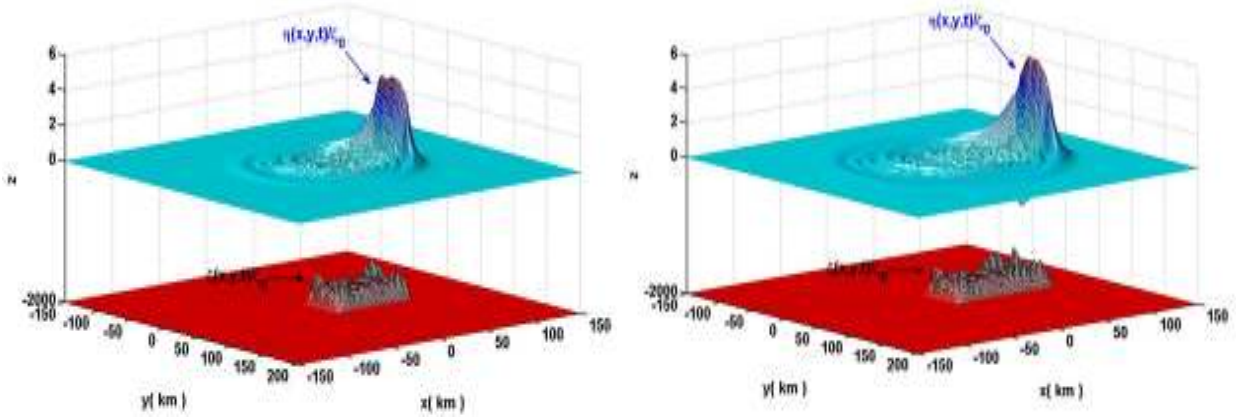

(c) $t = 0.75\ t^*$ (d) $t = \ t^*$

Fig. 3: Generation of the normalized tsunami waveforms, $\frac{\eta(x,y,t)}{\zeta_0}$, for a sample trajectory of the stochastic source model at different rise times with $\sigma = 1$, $L = 100\ km$, $D = 50\ km$, $t^* = \frac{L}{v}$ and $v = v_t$

This amplification occurs above the source progressively, as the source evolves, by adding uplifted fluid to the fluid displaced previously by uplifts of preceding source segments. As the spreading length in the fault increases, the amplitude of the tsunami wave increases. Moreover, it can be observed from Fig. 5, that at $t = 0.5\,t^*$, the deterministic waveform is in complete agreement with the aspect of the tsunami generated by a slowly spreading uplift of the ocean bottom presented by Todorovska and Trifunac (2001) who considered a very simple kinematic source model on the form of Heaviside step function.

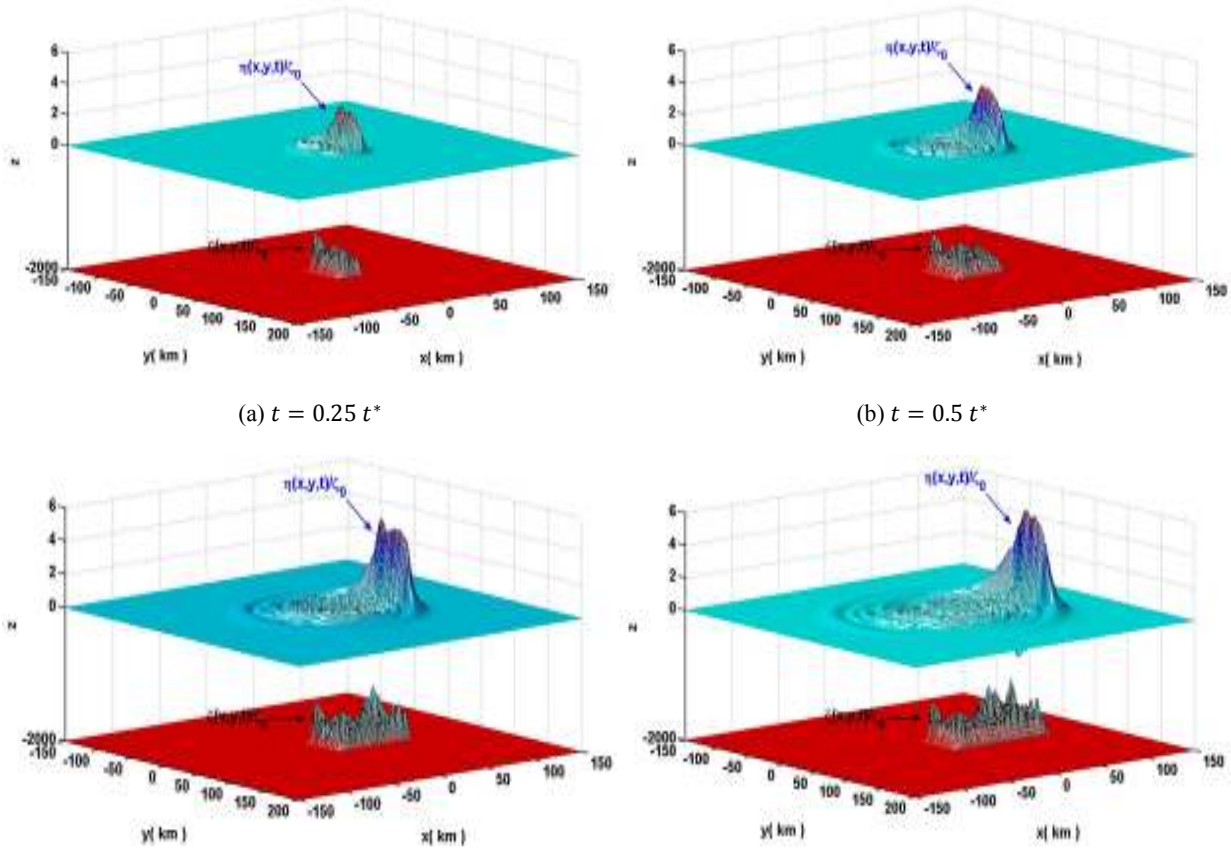

(a) $t = 0.25\,t^*$ (b) $t = 0.5\,t^*$

(c) $t = 0.75\,t^*$ (d) $t = t^*$

Fig. 4: Generation of the normalized tsunami waveforms, $\frac{\eta(x,y,t)}{\zeta_0}$, for the same trajectory of the stochastic source model at different rise times with $\sigma = 2$, $L = 100\ km$, $D = 50\ km$, $t^* = \frac{L}{v}$ and $v = v_t$

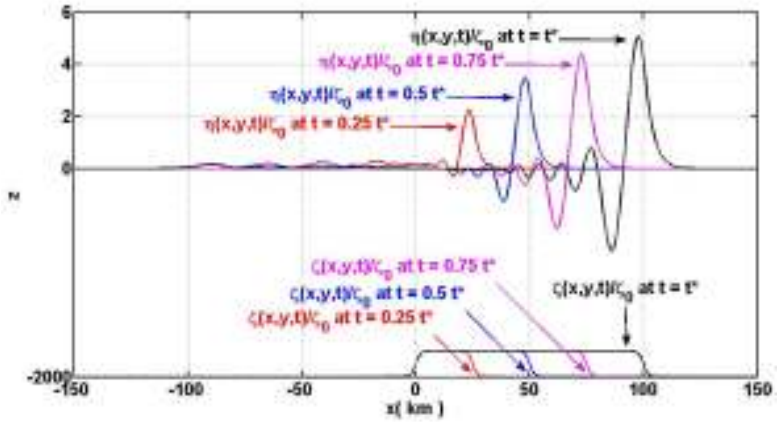

(a) $\sigma = 0$ (deterministic case)

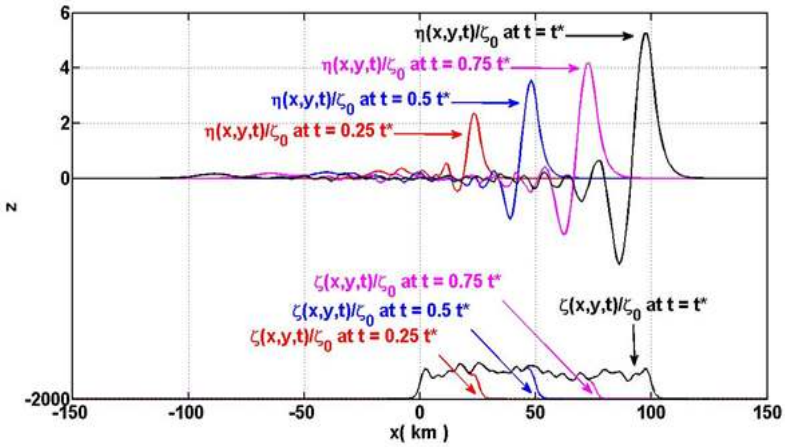

(b) $\sigma = 1$

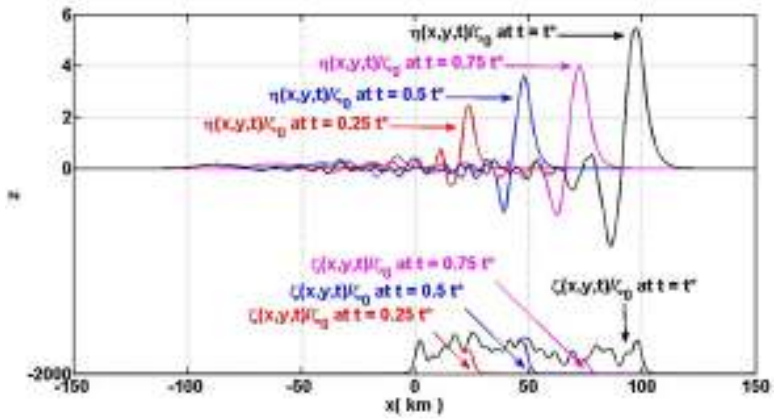

(c) $\sigma = 2$

Fig. 5: Side view of the generated normalized tsunami waveforms, $\frac{\eta(x,y,t)}{\zeta_0}$, for the same trajectory of the stochastic source model at different rise times with noise intensities $\sigma = 0, 1$ and 2, $L = 100\ km$, $D = 50\ km$, $v = v_t$ and $t^* = \frac{L}{v}$

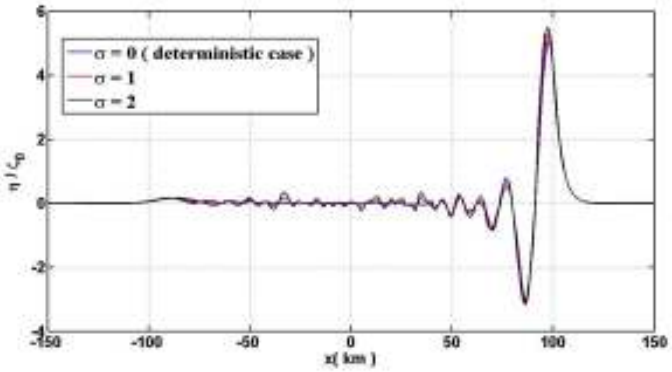

Fig. 6: Effect of the normalized noise intensity σ on the generation of tsunami waveforms for the same trajectory of the stochastic source model with $L = 100\ km$ and $D = 50\ km$ for $t = t^* = \frac{L}{v}$

Effect of normalized noise intensity σ on tsunami generation waveform: We studied the effect of the normalized noise intensity σ on the tsunami generation in Fig. 2 to 4. It can be observed from these figures that the increase in the normalized noise intensity leads to an increase in the deformation in the bottom

topography, while the wave behavior is mainly the same. Figure 6 present a collection of the waveforms from Fig. 5 at $t = t^*$ to get a better insight of the effect of the normalized noise intensity on the tsunami generation, where it can be observed that the increase of the normalized noise intensities on the bottom topography leads to slight difference in the peak amplitude of the waveforms in addition an increase in oscillations in the free surface elevation. These differences can be further investigated by discussing the variance of the generated tsunami waveforms. We investigated the normalized variance $(\frac{Var}{\sigma^2})$ of the tsunami generation in Fig. 7 and 8 at $h = 2\ km$, $L = 100\ km, D = 50\ km$ at time $t = 0.25\ t^*, 0.5\ t^*,$ $0.75\ t^*$ and t^*. It can be seen in Fig. 8 that the variance increases with the increase in time and the maximum amplitude of the variance occurs above the spreading edge of the bottom topography. The maximum variance occurs at $t = t^*$ (maximum amplification of the wave). Thus we can conclude that the variance and the tsunami waveforms behave similarly during the generation process under the effect of the normalized noise intensities which is also clear in Fig. 7.

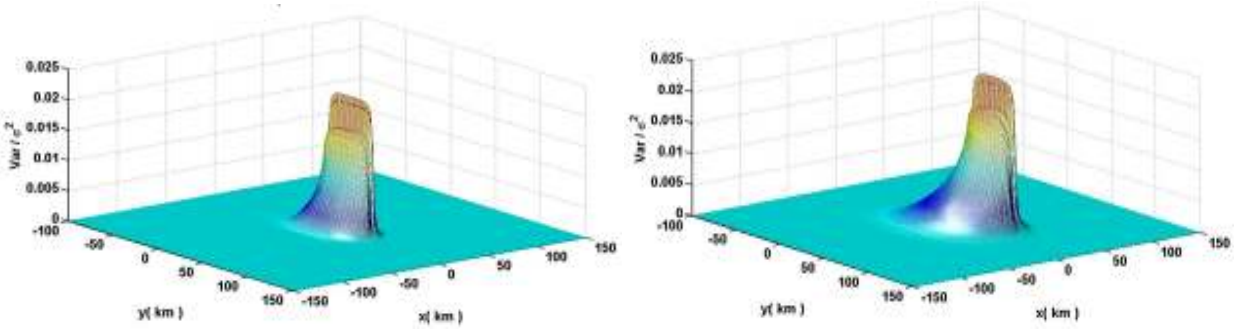

(a) $t = 0.25\ t^*$ (b) $t = 0.5\ t^*$

(c) $t = 0.75\ t^*$ (d) $t = t^*$

Fig. 7: Normalized wave dispersion (variance) of the tsunami generation at different time evolution for $h = 2\ km$ with $L = 100\ km$ and $D = 50\ km$

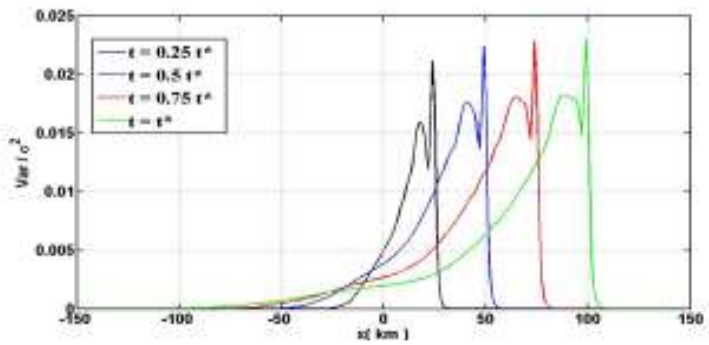

Fig. 8: Side view of the normalized wave dispersion of the tsunami generation at different time evolution for $h = 2\ km$ with $L = 100\ km$ and $D = 50\ km$

Time evolution during tsunami propagation: The effects of variations of the faulting on the propagation of tsunami wave, after the completion of the formation of the stochastic source model, are studied as a function of time t. These effects are studied through the investigation of the propagation of tsunami wave under the effect of the normalized noise intensity σ. Figure 9 and 10 illustrate the propagation process of the mean and the variance of tsunami propagation waveforms, respectively, in the far-field for times $t = 2\ t^*, 3\ t^*, 4\ t^*$, where $t^* = \frac{L}{v}$ and $v = v_t$. It can be seen from these figures that the maximum wave amplitude decreases with time, due to the geometric spreading and also due to dispersion, causing a train of small waves behind the main wave. It can be seen from Fig. 8 that the amplitude of the leading normalized mean decreases from 1.775 at $t = 2\ t^*$ to 0.7424 at $t = 4\ t^*$, while from Fig. 9 the amplitude of the leading normalized variance decreases from 0.000654 at $t = 2\ t^*$ to 0.000111 at $t = 4\ t^*$.

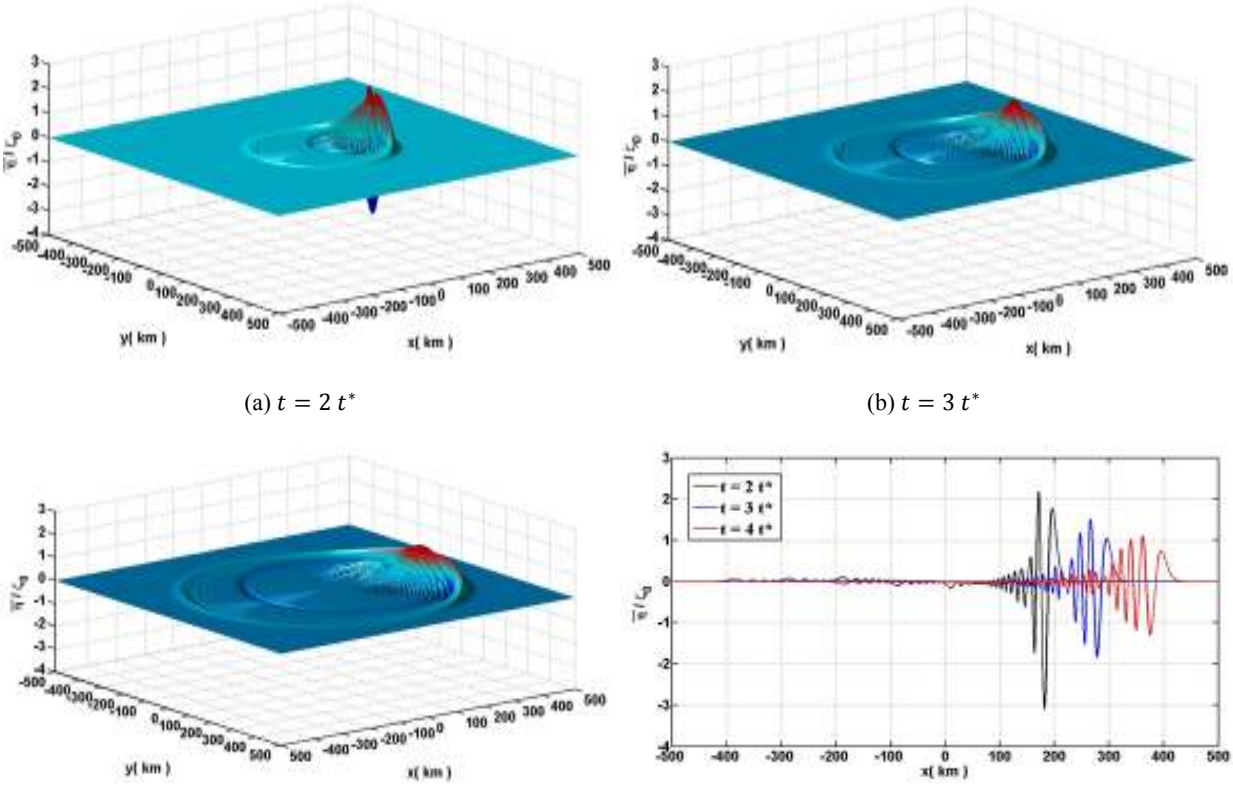

(a) $t = 2\ t^*$ (b) $t = 3\ t^*$

(c) $t = 4\ t^*$ (d) Side view at $t = 2\ t^*, 3\ t^*, 4\ t^*$

Fig. 9: The normalized mean of the propagated tsunami waveforms at different propagation times for propagated uplift length $L = 100\ km$, width $D = 50\ km$ $h = 2\ km$ at $t = 2\ t^*$, $3\ t^*$, $4\ t^*$ where $t^* = \frac{L}{v}$ and $v = v_t$

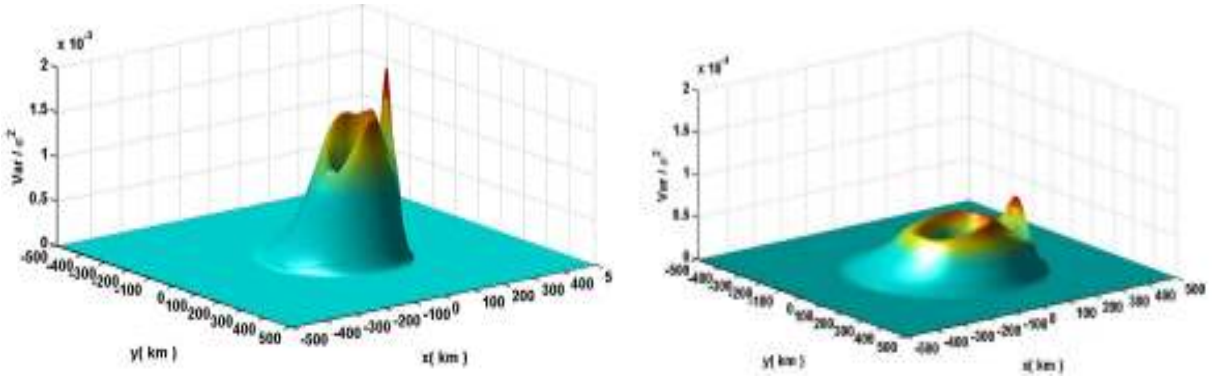

(a) $t = 2\ t^*$ (b) $t = 3\ t^*$

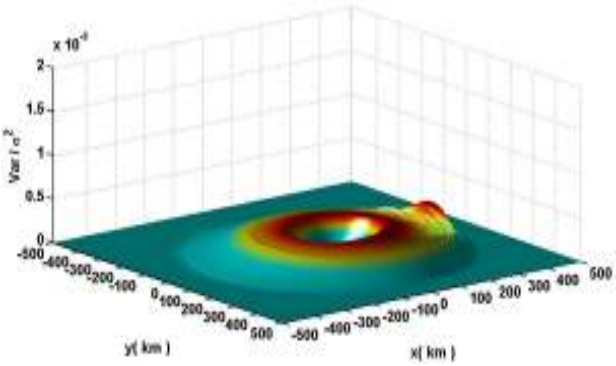

(c) $t = 4\ t^*$

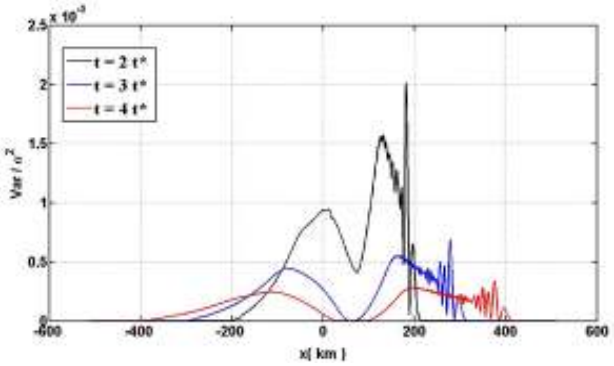

(d) Side view at $t = 2\ t^*, 3\ t^*, 4\ t^*$

Fig. 10: The normalized variance of the propagated tsunami waveforms at different propagation times for propagated uplift length $L = 100\ km$, width $D = 50\ km$ $h = 2\ km$ at $t = 2\ t^*$, $3\ t^*$, $4\ t^*$ where $t^* = \frac{L}{v}$ and $v = v_t$

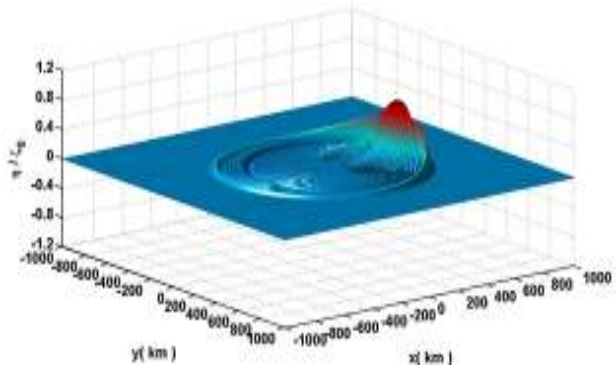

(a) $t = 4\ t^*$

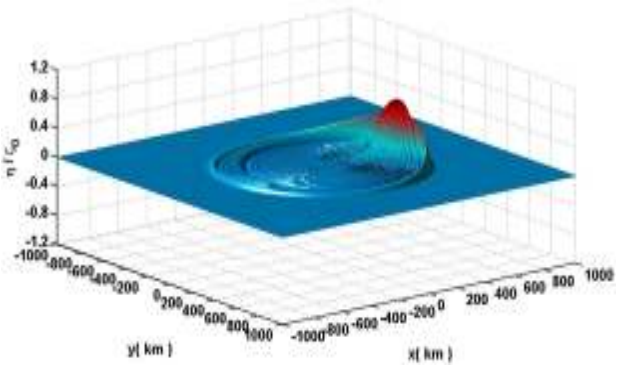

(b) $t = 6\ t^*$

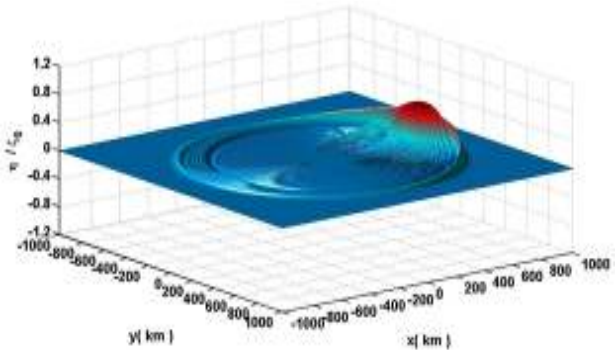

(c) $t = 8\ t^*$

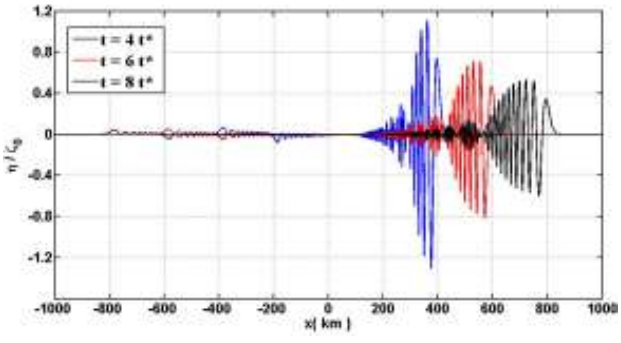

(d) Side view at $t = 4\ t^*, 6\ t^*, 8\ t^*$

Fig. 11: Propagation of the normalized tsunami waveforms, $\frac{\eta(x,y,t)}{\zeta_0}$, for different rise times at $\sigma = 0$, $L = 100\ km$, $D = 50\ km$, $v = v_t$ and $t^* = \frac{L}{v}$

Effect of normalized noise intensities σ on tsunami propagation waveform: Figure 11 to 13 illustrate the propagation tsunami waveforms away from the stochastic source model presented in Fig. 1 to 3, respectively at noise intensity $\sigma = 0$, 1 and 2. These waveforms are the propagation of the generated tsunami waveforms represented in Fig. 6 at propagated times $t = 4\ t^*$, $6\ t^*$ and $8\ t^*$ where $t^* = \frac{L}{v}$ and $v = v_t$. It can be seen from these figures that the maximum wave amplitude decreases during the time evolution due to geometric spreading and due to dispersion for noise intensities $\sigma = 0$, 1 and 2. It can be observed

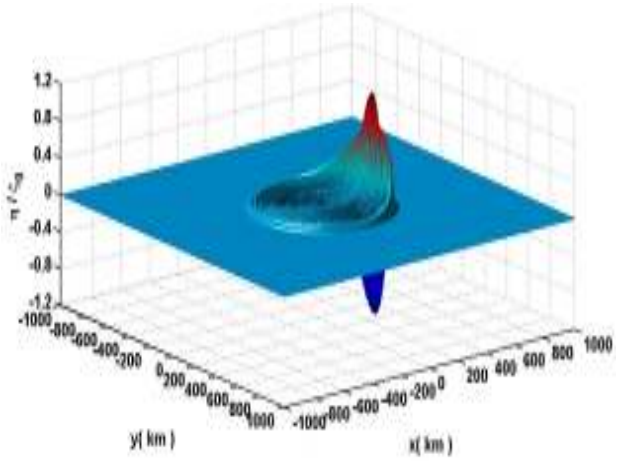

(a) $t = 4\ t^*$

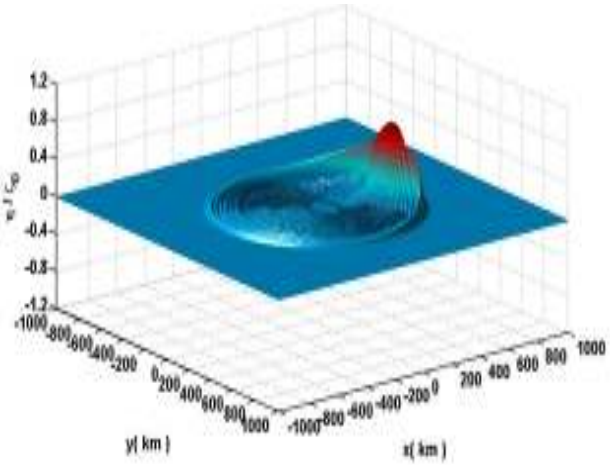

(b) $t = 6\ t^*$

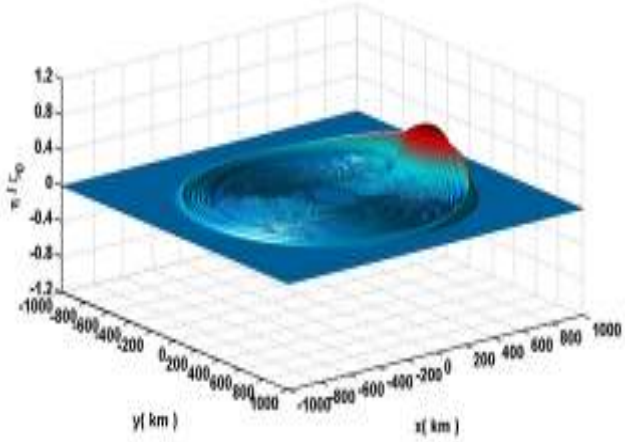

(c) $t = 8\ t^*$

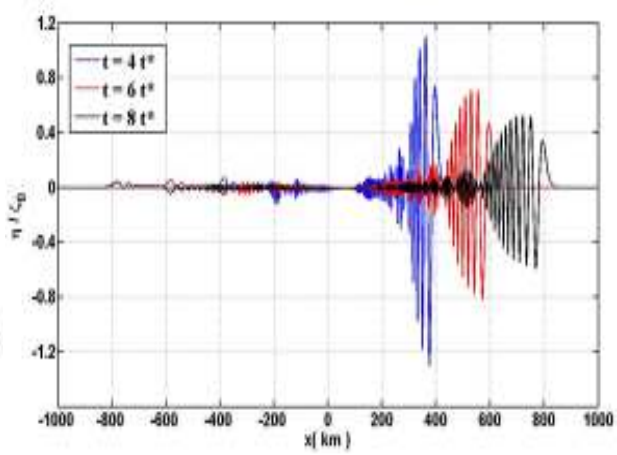

(d) Side view at $t = 4\ t^*, 6\ t^*, 8\ t^*$

Fig. 12: Propagation of the normalized tsunami waveforms, $\frac{\eta(x,y,t)}{\zeta_0}$, for the same trajectory of the stochastic source model at different rise times with $\sigma = 1$, $L = 100\ km$, $D = 50\ km$, $v = v_t$ and $t^* = \frac{L}{v}$

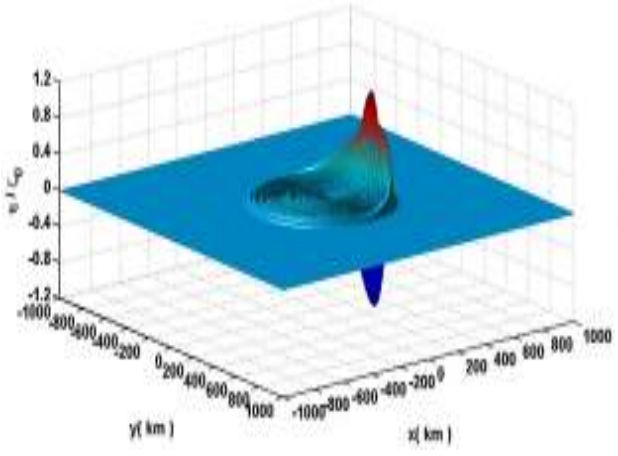

(a) $t = 4\ t^*$

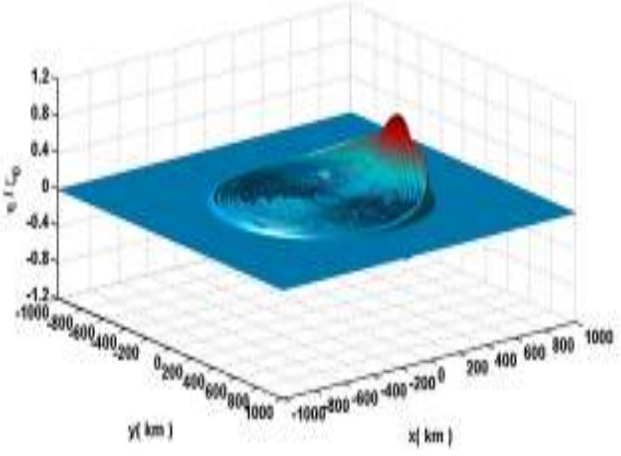

(b) $t = 6\ t^*$

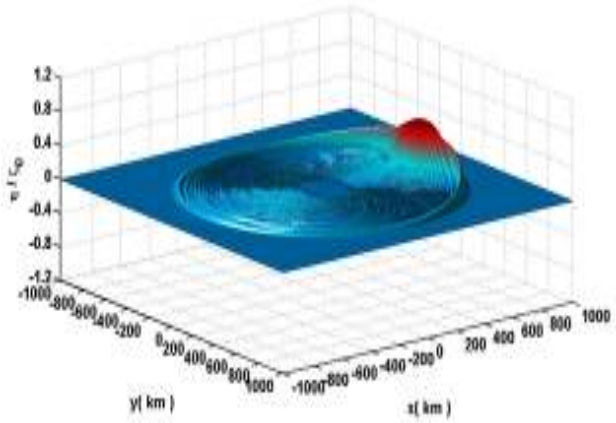

(c) $t = 8\ t^*$

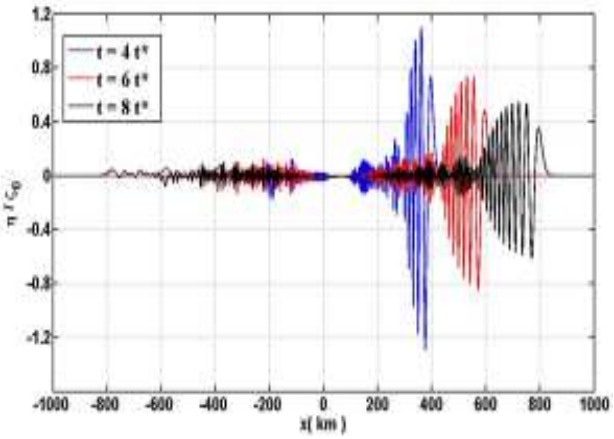

(d) Side view at $t = 4\ t^*, 6\ t^*, 8\ t^*$

Fig. 13: Propagation of the normalized tsunami waveforms, $\frac{\eta(x,y,t)}{\zeta_0}$, for the same trajectory of the stochastic source model at different rise times with $\sigma = 2$, $L = 100\ km$, $D = 50\ km$, $v = v_t$ and $t^* = \frac{L}{v}$

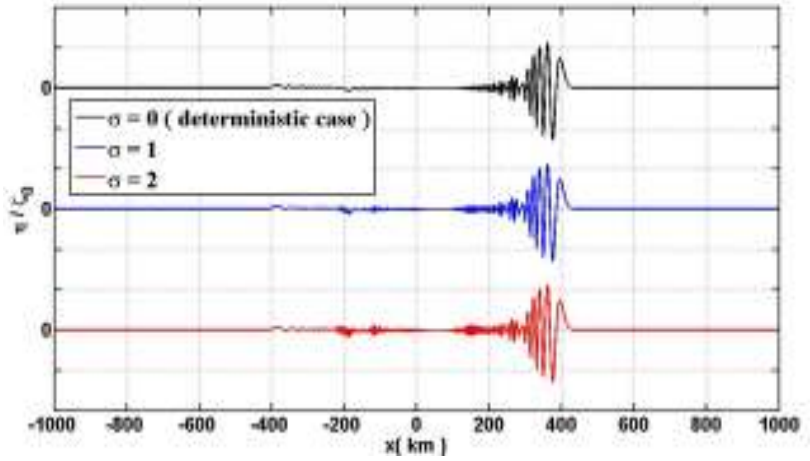

(a) $t = 4\ t^*$

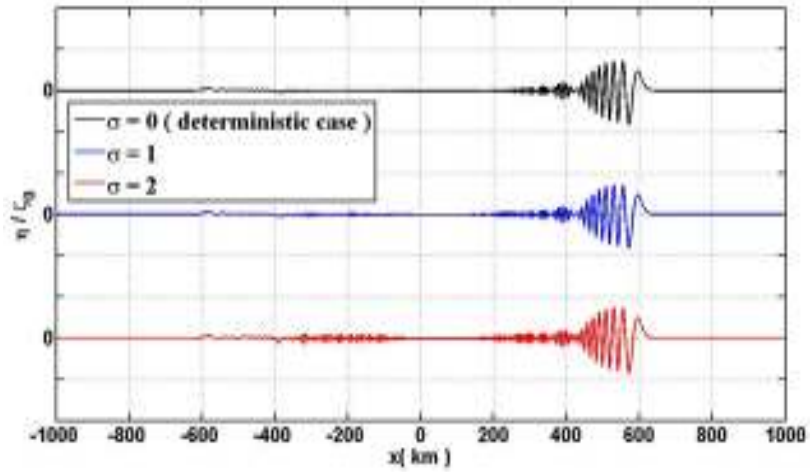

(b) $t = 6\ t^*$

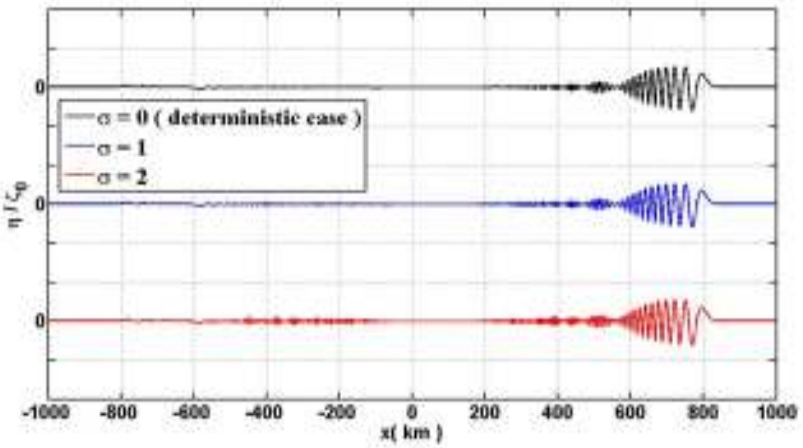

(c) $t = 8\ t^*$

Fig. 14: Effect of the normalized noise intensity σ on the propagation of tsunami waveforms for the same trajectory of the stochastic source model with, $L = 100\ km$, $D = 50\ km$ for different propagation times t where $t^* = \frac{100}{v}$

from Fig. 14 that the increase of the normalized noise intensity leads to an increase in oscillations and more dispersion in the normalized free surface elevation but leads to a slight difference in the peak amplitude of the waveforms.

CONCLUSION

In this study, the process of tsunami generation and propagation was investigated over a stochastic bottom topography represented by a sliding Heaviside step function under the influence of two independent Gaussian white noise processes in the $x-$ and $y-$directions, respectively. We demonstrated the waveform amplification resulting from stochastic source spreading and wave focusing in the near-field and the tsunami propagation in the far-field. Due to the stochastic nature of the bottom topography, the free surface elevation becomes a stochastic process having infinite number of trajectories (realizations). Therefore we derived mathematically the mean and variance of the stochastic tsunami waveforms and illustrated them graphically to get a better insight of the overall behavior of the stochastic tsunami waveforms under the effect of the noise intensity. It was observed that near the source, the wave has large amplitude as the wave builds up progressively as t increases and the focusing and the amplification of tsunami amplitudes occur above the spreading edge of the stochastic source model, while as the tsunami further departed away from the source the amplitude decreased due to dispersion. Moreover, the maximum dispersion (variance) was found to occur at the corresponding maximum or minimum amplitude of mean generated wave. Also, when increasing the normalized noise intensity, the oscillations of the free surface elevation increase. In addition to an increase in the difference in the peak amplitudes of the waveforms, especially the leading wave, while in the propagation process, it was observed that the increase in the noise intensity show more dispersion and oscillation in the propagated free surface elevation.

REFERENCES

Abou-Dina, M.S. and F.M. Hassan, 2006. Generation and propagation of nonlinear tsunamis in shallow water by a moving topography. Appl. Math. Comput., 177: 785-806.

Craig, W., P. Guyenne and C. Sulem, 2009. Water waves over a random bottom. J. Fluid Mech., 640: 79-107.

De Bouard, A., W. Craig, O. DDíaz-Espinosa, P. Guyenne and C. Sulem, 2008. Long wave expansions for water waves over random topography. Nonlinearity, 21(9): 2143.

Dutykh, D. and F. Dias, 2007. Water waves generated by a moving bottom. Tsunami Nonlinear Waves, pp: 65-95.

Dutykh, D., F. Dias and Y. Kervella, 2006. Linear theory of wave generation by a moving bottom. C. R. Math., 343: 499-504.

Dutykh, D., C. Labart and D. Mitsotakis, 2011. Long wave runup on random beaches. Phys. Rev. Lett., 107(2011): 184504.

Geist, E.L., 2002. Complex earthquake rupture and local tsunamis. J. Geophys. Res., 107: 2086-2100.

Geist, E.L., 2005. Rapid tsunami models and earthquake source parameters: Far-field and local applications. ISET J. Earthquake Technol., 42(4): 127-136.

Gurevich, B., A. Jeffrey and E. Pelinovsky, 1993. A method for obtaining evolution equations for nonlinear waves in a random medium. Wave Motion, 17(5): 287-295.

Hammack, J.L., 1973. A note on tsunamis: Their generation and propagation in an ocean of uniform depth. J. Fluid Mech., 60: 769-799.

Hassan, F.M., 2009. Boundary integral method applied to the propagation of non-linear gravity waves generated by a moving bottom. Appl. Math. Model., 33: 451-466.

Hassan, H.S., K.T. Ramadan and S.N. Hanna, 2010a. Generation and propagation of tsunami by a moving realistic curvilinear slide shape with variable velocities in linear zed shallow-water wave theory. Engineering, 2(7): 529-549.

Hassan, H.S., K.T. Ramadan and S.N. Hanna, 2010b. Numerical solution of the rotating shallow water flows with topography using the fractional steps method. Appl. Math., 1(2): 104-117.

Hayir, A., 2003. The effects of variable speeds of a submarine block slide on near-field tsunami amplitudes. Ocean Eng., 30(18): 2329-2342.

Kanamori, H. and G.S. Stewart, 1972. A slowly earthquake. Phys. Earth Planet. In., 18: 167-175.

Kervella, Y., D. Dutykh and F. Dias, 2007. Comparison between three-dimensional linear and nonlinear tsunami generation models. Theor. Comp. Fluid Dyn., 21: 245-269.

Klebaner, F.C., 2005. Introduction to Stochastic Calculus with Application. 2nd Edn., Imperial College Press, London.

Kloeden, P.E. and E. Platen, 1992. Numerical Solution of Stochastic Differential Equations. Springer, Berlin.

Manouzi, H. and M. Seaïd, 2009. Solving wick-stochastic water waves using a galerkin finite element method. Math. Comput. Simulat., 79: 3523-3533.

Nachbin, A., 2010. Discrete and continuous random water wave dynamics. Discrete Cont. Dyn. S. (DCDS-A), 28(4): 1603-1633.

Nakamura, S., 1986. Estimate of exceedance probability of tsunami occurrence in the eastern pacific. Mar. Geod., 10(2): 195-209.

Oksendal, B., 1995. Stochastic Differential Equations: An Introduction with Applications. 5th Edn., Springer, Berlin.

Omar, M. A., A. Aboul-Hassan and S.I. Rabia, 2009. The composite Milstein methods for the numerical solution of Stratonovich stochastic differential equations. Appl. Math. Comput., 215(2): 727-745.

Omar, M.A., A. Aboul-Hassan and S.I. Rabia, 2011. The composite Milstein methods for the numerical solution of Itô stochastic differential equations. J. Comput. Appl. Math., 235(8): 2277-2299.

Ramadan, K.T., H.S. Hassan and S.N. Hanna, 2011. Modeling of tsunami generation and propagation by a spreading curvilinear seismic faulting in linearized shallow-water wave theory. Appl. Math. Model., 35(1): 61-79.

Ramadan, K.T., M.A. Omar and A.A. Allam, 2014. Modeling of tsunami generation and propagation under the effect of stochastic submarine landslides and slumps spreading in two orthogonal directions. Ocean Eng., 75: 90-11

Rascón, O.A. and A.G. Villarreal, 1975. On a stochastic model to estimate tsunami risk. J. Hydraul. Res., 13(4): 383-403.

Silver, P.G. and T.H. Jordan, 1983. Total-moment spectra of fourteen large earthquakes. J. Geophys. Res., 88: 3273-3293.

Titov, V. V. and C. Synolakis, 1995. Modeling of breaking and nonbreaking long-wave evolution and runup using vtcs-2. J. Waterw. Port C-ASCE, 121(6): 308-317.

Todorovska, M.I. and M.D. Trifunac, 2001. Generation of tsunamis by a slowly spreading uplift of the sea floor. Soil Dyn. Earthq. Eng., 21: 151-167.

Todorovska, M.I., A. Hayir and M.D. Trifunac, 2002. A note on tsunami amplitudes above submarine slides and slumps. Soil Dyn. Earthq. Eng., 22(2): 129-141.

Trifunac, M.D. and M.I. Todorovska, 2002. A note on differences in tsunami source parameters for submarine slides and earthquakes. Soil Dyn. Earthq. Eng., 22(2): 143-155.

Trifunac, M.D., A. Hayir and M.I. Todorovska, 2002a. A note on the effects of nonuniform spreading velocity of submarine slumps and slides on the near-field tsunami amplitudes. Soil Dyn. Earthq. Eng., 22(3): 167-180.

Trifunac, M.D., A. Hayir and M.I. Todorovska, 2002b. Was grand banks event of 1929 a slump spreading in two directions. Soil Dyn. Earthq. Eng., 22(5): 349- 360.

Wiegel, R.L., 1970. Earthquake Engineering. Prentice-Hall, Englewood Cliffs, New Jersey.

Zahibo, N., E. Pelinovsky, T. Talipova, A. Kozelkov and A. Kurkin, 2006. Analytical and numerical study of nonlinear effects at tsunami modeling. Appl. Math. Comput., 174(2): 795-809.